Author(s): Chivers, Tristram; Eisler, Dana; Fedorchuk, Chantall; Schatte, Gabriele; Tuononen, Heikki

Title: Syntheses and Structures of Magnesium and Zinc Boraamidinates: EPR and DFT Investigations of Li, Mg, Zn, B, and In Complexes of the [PhB(NtBu)2]•- Anion Radical

Year: 2006

Version:

Please cite the original version:

Chivers, T., Eisler, D., Fedorchuk, C., Schatte, G., & Tuononen, H. (2006). Syntheses and Structures of Magnesium and Zinc Boraamidinates: EPR and DFT Investigations of Li, Mg, Zn, B, and In Complexes of the [PhB(NtBu)2]•- Anion Radical. Inorganic Chemistry, 45(5), 2119-2131. https://doi.org/10.1021/ic0520014

Syntheses and Structures of Magnesium and Zinc Boraamidinates: EPR and DFT Investigations of Li, Mg, Zn, B, and In Complexes of the $[PhB(N^tBu)_2]^{-\bullet}$ Anion Radical

Tristram Chivers,* Dana J. Eisler, Chantall Fedorchuk, Gabriele Schatte, and Heikki M. Tuononen

Department of Chemistry, University of Calgary, Calgary, Alberta, Canada T2N 1N4.

René T. Boeré

Department of Chemistry and Biochemistry, University of Lethbridge, Lethbridge, Alberta, Canada T1K 3M4.

* To whom correspondence should be addressed.
Telephone: (403) 220-5741
Fax: (403) 289-9488
E-mail: chivers@ucalgary.ca

Abstract

The first magnesium and zinc boraamidinate (*bam*) complexes have been synthesized *via* metathetical reactions between dilithio *bam*s and Grignard reagents or MCl_2 (M = Mg, Zn). The following new classes of *bam* complexes have been structurally characterized: the heterobimetallic spirocycles $\{(L)\mu\text{-Li}[PhB(\mu\text{-N}^t\text{Bu})_2]\}_2M$ (**6a** or **6b**, M = Mg, L = Et_2O or THF; **6c**, M = Zn, L = Et_2O), bis(organomagnesium) complexes $\{[PhB(\mu_3\text{-N}^t\text{Bu})_2](Mg^t\text{Bu})_2(\mu_3\text{-Cl})Li(OEt_2)_3\}$ (**8**) and $\{[PhB(\mu_3\text{-N}^t\text{Bu})_2](MgR)_2(THF)_2\}$ (**9a**, R = ^{i}Pr; **9b**, R = Ph), and the mononuclear complex $\{[PhB(\mu\text{-NDipp})_2]Mg(OEt_2)_2\}$ (**10**). Oxidation of **6a** or **6c** with iodine produces persistent pink (**16a**, M = Mg) or purple (**16b**, M = Zn) neutral radicals $\{L_x\mu\text{-Li}[PhB(\mu\text{-N}^t\text{Bu})_2]_2M\}^\bullet$ (L = solvent molecule), which are shown by EPR spectra supported by DFT calculations to be C_s-symmetric species with spin density localized on one of the *bam* ligands. In contrast, characterization of the intensely colored neutral radicals $\{[PhB(\mu\text{-N}^t\text{Bu})_2]_2M\}^\bullet$ (**5c**, M = In, dark green; **5d**, M = B, dark purple) reveals that the spin density is equally delocalized over all four nitrogen atoms in these D_{2d}-symmetric spirocyclic systems. Oxidation of the dimeric dilithio complex $\{Li_2[PhB(\mu_4\text{-N}^t\text{Bu})_2]\}_2$ with iodine produces the monomeric neutral radical $\{[PhB(\mu\text{-N}^t\text{Bu})_2]Li(OEt_2)_x\}^\bullet$ (**17**), characterized by EPR spectra and DFT calculations. These findings establish that the *bam* anionic radical $[PhB(N^t\text{Bu})_2]^{-\bullet}$ can be stabilized by coordination to a variety of early main-group metal centers to give neutral radicals whose relative stabilities are compared and discussed.

Introduction

The coordination chemistry of the monoanionic amidinate (*am*) ligand $[RC(NR')_2]^-$ (Chart 1) has been extensively studied.[1] For example, *am* complexes of all the *s*-block elements have been reported.[1] In the context of the current work, a variety of magnesium *am* complexes have been identified. These include mono- and bis-*am* complexes of the general formulae $[RC(\mu\text{-}NR')_2]MgX$ and $[RC(\mu\text{-}NR')_2]_2Mg$ (R, R' = alkyl, aryl, $SiMe_3$; X = alkyl, aryl, halide)[2] in which the Mg centers are usually stabilized by a Lewis base. In addition, dinuclear Mg complexes with bridging *am*s {$[RC(\mu\text{-}NR')_2][\mu\text{-}RC(NR')_2\kappa^2\textit{N,N'}]Mg\}_2$,[2d,3] complexes involving pendant *am*s,[4] and mixed Mg/Al mono-*am* complexes $\{[MeC(\mu\text{-}NR')_2][Me_2Al(\mu\text{-}N^iPr)_2]Mg\}$ have been reported.[5] Potential applications of Mg *am* complexes include their use as reagents for the synthesis of transition-metal complexes and in chemical vapour deposition (CVD). Group 13 *am* complexes are also of interest as potential single-source precursors to nitride materials and as selective reagents and catalysts. The most important classes include mono-*am* complexes $[RC(\mu\text{-}NR')_2]MX_2$ (M = Group 13 element; R, R' = alkyl, aryl, $SiMe_3$; X = halide, hydride, alkyl, aryl),[6] bis-*am* complexes $[RC(\mu\text{-}NR')_2]_2MX$,[6b,6f,7] tris-*am* complexes $[RC(\mu\text{-}NR')_2]_3M$,[6f,8] dinuclear Group 13 complexes with bridging *am* ligands, and complexes of the type $\{[\mu\text{-}RC(NR')_2\kappa^2\textit{N,N'}]MX_2\}_2$ and $\{[\mu\text{-}RC(NR')_2\kappa^2\textit{N,N'}]_2MX\}_2$,[6f,9] incorporating pendant *am*s.[4a,10]

By comparison, the coordination chemistry of the dianionic boraamidinate (*bam*) ligand $[RB(NR')_2]^{2-}$ (isoelectronic with *am*, Chart 1) is still in its infancy. For *s*-block metal complexes, only lithium derivatives have been reported.[11] These reagents have provided the predominant method of transferring the *bam* ligand to other metal centers.[11e]

The first X-ray structural determinations of dilithio *bam* complexes have shown that the extent of aggregation is influenced by the substituent (R) on boron, where the fundamental building block is the Li_2N_2B unit **A** (Chart 1).[11b,11c] In the case of the dimers $\{Li_2[RB(\mu_4\text{-}N^tBu)_2]\}_2$ (**1a**, R = Ph; **1b**, ^{n}Bu; **1c**, ^{t}Bu), two of these units participate in a face-to-face interaction through lithium–nitrogen contacts to give the bicapped cube **B**. In the unique example of a trimer $\{Li_2[RB(\mu_4\text{-}N^tBu)_2]\}_3$ (**2**, R = Me), three Li_2N_2B units associate edge-on through lithium–nitrogen contacts to give the tricapped hexagonal prism **C**. The solvated complex $\{(THF)_2(\mu\text{-}THF)Li_2[PhB(\mu_3\text{-}NDipp)_2]\}$ (**3**) (Chart 1)[11d] is an unique example of a monomeric dilithio boraamidinate. An intriguing observation during investigations of the dilithio *bam* complexes **1a–c** was the formation of red solutions upon exposure to air or during the course of metathetical reactions with main-group element halides.[11c] In related polyimido anions of *p*-block elements, such behavior is associated with the formation of free radicals.[12]

Chart 1.

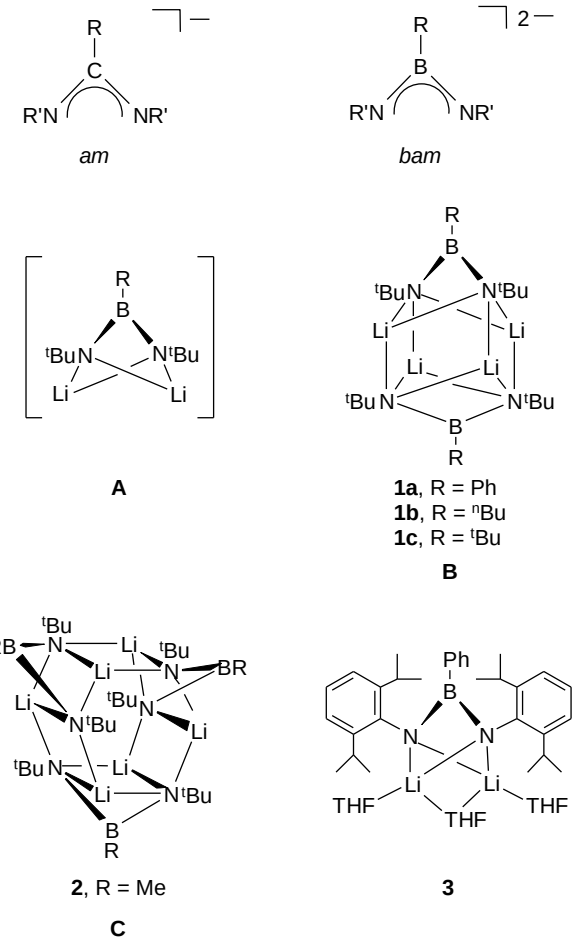

Until 1993, reports on *p*-block *bam* derivatives were restricted to Groups 14–16,[11a,11c,11e,13] with the exception of {[μ-Mes*B(NMe)$_2\kappa^2$*N,N'*]AlMe}$_2$ for which a crystal structure has not been reported.[13i] Early investigations of the coordination chemistry of the *bam* dianion with transition metals were limited to Group 4,[11a,14] but recently, Nocera and co-workers have described complexes of Groups 5 and 6 including octahedral tris-*bam* complexes and a paramagnetic vanadium(IV) complex.[15] We have described the characterization of the spirocyclic anions {[PhB(μ-N^{t}Bu)$_2$]$_2$M}$^-$ (**4a**, M = Al, **4b**, M = Ga; **4c**, M = In) as their lithium derivatives[16,17] and showed that the oxidation

of **4a** and **4b** with iodine produces stable[18] neutral radicals {[PhB(μ-N^{t}Bu)$_2$]$_2$M}$^\bullet$ (**5a**, M = Al; **5b**, M = Ga), which were characterized in the solid state by X-ray crystallography. A combination of EPR spectroscopic analyses and DFT calculations showed that spin delocalization is uniform over both *bam* ligands in **5a** and **5b** and that the spirocyclic structure is retained in solution (Scheme 1).[17]

Scheme 1.

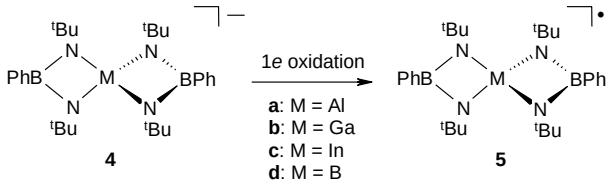

Herein, we describe studies that extend the coordination chemistry of the *bam* ligand to magnesium and zinc. The synthesis and characterization of a series of magnesium *bam*s, including the heterobimetallic spirocyclic complexes {(Et$_2$O)μ-Li[PhB(μ-N^{t}Bu)$_2$]}$_2$M (**6a**, M = Mg; **6c**, M = Zn), are discussed. The oxidation of **6a** and **6c** with iodine produces persistent[18] radicals, which have been characterized by a combination of EPR spectra and DFT calculations. In addition, we have extended our earlier studies of Group 13 spirocyclic *bam* radicals {[PhB(μ-N^{t}Bu)$_2$]$_2$M}$^\bullet$ to the characterization of the indium- and boron-containing analogues (Scheme 1; **5c**, M = In; **5d**, M = B). Finally, we describe the identification of the paramagnetic red species formed upon oxidation of dilithio *bam*s.[11c]

Results and Discussion

Syntheses and Spectroscopic Characterization of Mg and Zn *bam*s. The reaction of $Li_2[PhB(\mu_3\text{-}N^tBu)_2]$ (**1a**) and a Grignard reagent in a 1:1 stoichiometry was attempted in an effort to generate the mixed-metal Mg/Li mono-*bam* **7** (Scheme 2, Method 1). However, the reaction with ^{t}BuMgCl affords the spirocyclic dilithio magnesium bis-*bam* complex $\{(Et_2O)\mu\text{-}Li[PhB(\mu\text{-}N^tBu)_2]\}_2Mg$ (**6a**, Scheme 2).

Scheme 2

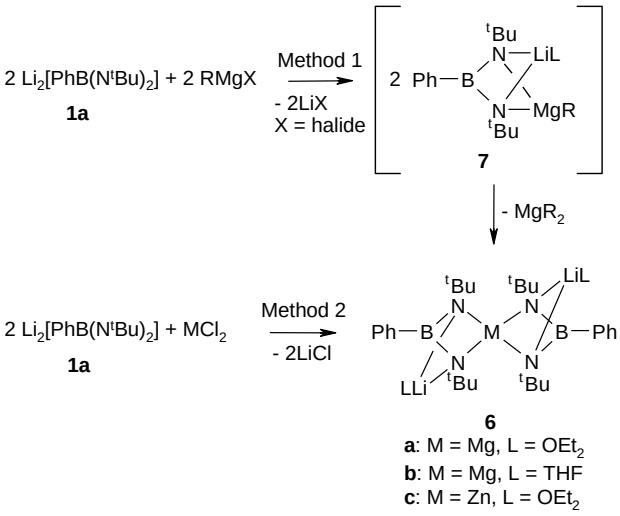

The proposed pathway involves the initial production of **7**, which then undergoes redistribution to produce **6a** (89 %) with the elimination of Mg^tBu_2 that was detected by ^{1}H NMR spectroscopy (~ δ 0.2). The generality of Method 1 (Scheme 2) was demonstrated in the reactions of **1a** with a variety of Grignard reagents in diethyl ether, including MesMgBr, ^{n}BuMgCl, and MeMgBr, all of which produce **6a**. Similarly, the THF derivative $\{(THF)\mu\text{-}Li[PhB(\mu\text{-}N^tBu)_2]\}_2Mg$ (**6b**) is obtained from the reactions of the Grignard reagents PhMgCl or ^{i}PrMgCl in THF and **1a** in a 1:1 stoichiometry.

Complexes of type **6** may also be prepared by a direct approach (Method 2, Scheme 2). Treatment of two eq. of **1a** with MCl_2 (M = Mg or Zn) in diethyl ether at –78 °C afforded **6a** and the zinc analogue $\{(Et_2O)\mu\text{-Li}[PhB(\mu\text{-N}^t\text{Bu})_2]\}_2Zn$ (**6c**) in 75 and 51 % yields, respectively. Colorless crystals of **6a** and **6c**, grown from concentrated solutions in Et_2O, were characterized by CHN analyses, ^1H, ^{11}B, ^7Li, and ^{13}C NMR spectra, and X-ray structural analyses (*vide infra*). For both **6a** and **6c**, the ^1H NMR spectra show resonances for the Ph and ^{t}Bu substituents and the coordinated Et_2O molecules in the appropriate relative intensities. However, the ^1H NMR spectrum for **6a** displays two singlets for the four ^{t}Bu groups attached to the amide nitrogens of the *bam*; consistently, two signals assigned to the methyl groups of these ^{t}Bu substituents are observed in the ^{13}C NMR spectrum. In contrast, only one ^{t}Bu resonance is observed in the ^1H NMR and ^{13}C NMR spectra for **6c**. The ^{11}B NMR spectra of **6a**–**c** exhibit broad resonances at δ 37-38, consistent with three-coordinate boron centers.[19] Singlets are observed in the ^7Li NMR spectra of **6a**–**c** at δ 1.44, 1.43 and 1.16, respectively.

When the reaction of **1a** and ^{t}BuMgCl was carried out in a 1:2 stoichiometry, colorless crystals of the bis(organomagnesium) complex $\{[PhB(\mu_3\text{-N}^t\text{Bu})_2](Mg^t\text{Bu})_2(\mu_3\text{-Cl})Li(OEt_2)_3\}$ (**8**, Scheme 3) were isolated. The ^1H NMR spectrum of **8** shows resonances for the Ph and ^{t}Bu substituents, along with the coordinated Et_2O molecules, in the appropriate relative intensities. The signals for the methyl groups of the two ^{t}Bu substituents attached to the amide nitrogen atoms appear at δ 1.44, while those on the two magnesium atoms are found at δ 1.12. The ^{11}B NMR resonance is observed at δ 39. A resonance is also observed at δ –0.37 in the ^7Li NMR spectrum of **8** consistent with the presence of LiCl in this complex.

Scheme 3

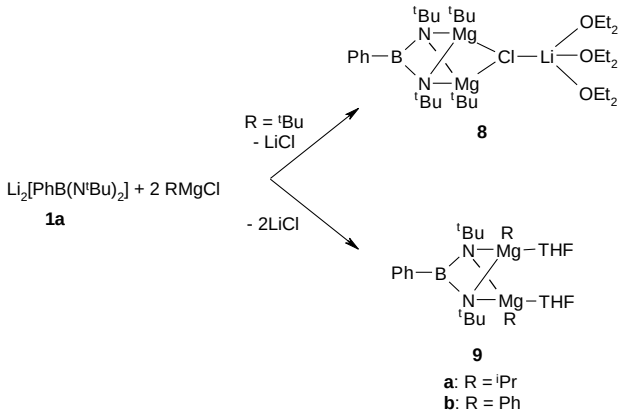

Treatment of **1a** with 2 eq. of solutions of ^{i}PrMgCl or PhMgCl in THF afforded {[PhB(μ_3-N^{t}Bu)$_2$](Mg^{i}Pr)$_2$(THF)$_2$} (**9a**) and {[PhB(μ_3-N^{t}Bu)$_2$](MgPh)$_2$(THF)$_2$} (**9b**), respectively (Scheme 3). The ^{1}H NMR spectrum of **9a** shows resonances for the Ph, ^{t}Bu, and ^{i}Pr substituents and coordinated THF molecules, with relative intensities indicative of symmetrical-equivalent ^{t}Bu and ^{i}Pr substituents and the presence of two coordinated THF molecules in solution. Similarly, the intensities of the resonances observed in the ^{1}H NMR spectrum of **9b** indicate three Ph groups, two ^{t}Bu substituents, and two coordinated THF molecules. The ^{11}B NMR chemical shifts for **9a** for **9b** are δ 39 and δ 40, respectively. No signals are observed in the ^{7}Li NMR spectra of **9a** and **9b**. Crystals of **9a** or **9b** suitable for X-ray structural determinations could not be obtained.

The reaction of PhB[N(H)Dipp]$_2$[11d] with $^{n/s}$Bu$_2$Mg (1:1) in boiling hexane produced the mono-*bam* complex {[PhB(μ-NDipp)$_2$]Mg(OEt$_2$)$_2$} (**10**, Scheme 4), which was identified by multinuclear NMR spectroscopy and an X-ray structural analysis (*vide infra*). The ^{1}H NMR spectrum of **10** exhibits only one resonance for both the CH and CH$_3$ groups of the Dipp substituents; the corresponding signals are observed in the ^{13}C

NMR spectrum. The ^{11}B NMR resonance of δ 31 for **10** is shifted upfield compared to those observed for **6**, **8**, and **9** (δ ^{11}B 37–40). Complete deprotonation was also indicated by the lack of an N–H stretch in the IR spectrum. For comparison, the reaction of $^{n/s}Bu_2Mg$ with *p*-tolylC[N(H)Dipp](NDipp) produces the *bis*-substituted square-planar complex [*p*-tolylC(μ-NDipp)$_2$]$_2$Mg.[2a]

Scheme 4

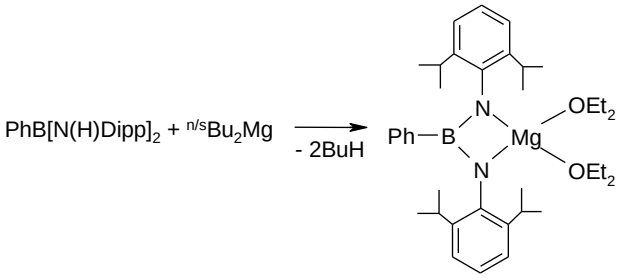

10

X-ray Structures of Mg and Zn *bam* Complexes. The X-ray structures of **6a** and **6c** show that the spirocyclic dianion {[PhB(μ-N^{t}Bu)$_2$]$_2$M}$^{2-}$ (M = Mg, Zn) is *N*,*N*'-chelated to two monosolvated lithium cations. The molecular geometry and atomic numbering scheme for **6a** and **6c** are shown in Figure 1, and pertinent structural parameters are summarized in Table 1. The two 4-membered NBNM (M = Mg, Zn) rings are puckered with the M and B atoms on one side of the plane, while the two four-coordinate nitrogen atoms reside on the other side of the plane.

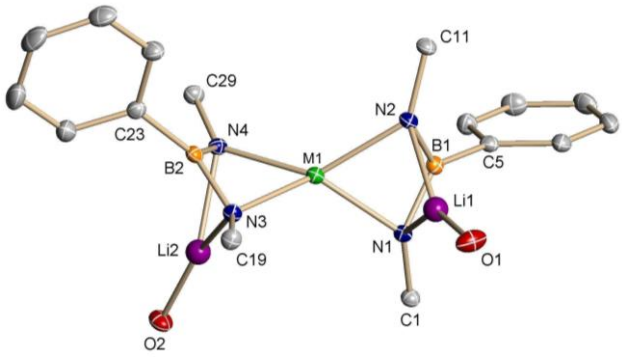

Figure 1. Thermal ellipsoid plot of {(Et_2O)μ-Li[PhB(μ-N^{t}Bu)$_2$]}$_2$M (M = Mg, **6a**; M = Zn, **6c**). For clarity, H atoms are omitted and only the α-carbons of the ^{t}Bu substituents and oxygen atoms of the Et_2O molecules are shown.

Table 1. Selected Bond Lengths (Å) and Bond Angles (°) for {(Et_2O)μ-Li[PhB(μ-N^{t}Bu)$_2$]}$_2$M (M = Mg, **6a**; M = Zn, **6c**).

	6a	**6c**		**6a**	**6c**
M(1)–N(1)	2.093(1)	2.076(4)	M(1)–N(3)	2.088(1)	2.024(4)
M(1)–N(2)	2.086(1)	2.013(4)	M(1)–N(4)	2.086(1)	2.067(4)
B(1)–N(1)	1.446(2)	1.436(8)	B(2)–N(3)	1.446(2)	1.443(7)
B(1)–N(2)	1.449(2)	1.443(7)	B(2)–N(4)	1.447(2)	1.425(7)
N(1)–Li(1)	2.023(3)	2.01(1)	N(3)–Li(2)	2.035(3)	2.07(1)
N(2)–Li(1)	2.033(3)	2.03(1)	N(4)–Li(2)	2.045(3)	2.03(1)
N(1)–M(1)–N(3)	125.45(5)	131.0(2)	N(2)–M(1)–N(1)	67.54(5)	68.4(2)
N(4)–M(1)–N(1)	138.54(5)	128.8(2)	N(2)–M(1)–N(3)	138.09(5)	136.6(2)
N(1)–B(1)–N(2)	106.7(1)	106.0(5)	N(3)–B(2)–N(4)	107.1(1)	106.9(4)
N(1)–B(1)–C(5)	126.7(1)	126.8(5)	N(3)–B(2)–C(23)	124.8(1)	126.5(5)

N(2)–B(1)–C(5)	126.6(1)	127.1(5)	N(4)–B(2)–C(23)	128.1(1)	126.5(5)
B(1)–N(1)–Li(1)	77.8(1)	78.3(4)	B(1)–N(2)–Li(1)	77.4(1)	77.5(4)
C(1)–N(1)–M(1)	132.21(9)	132.0(3)	C(11)–N(2)–M(1)	134.57(9)	132.3(3)
B(2)–N(3)–Li(2)	77.2(1)	77.5(4)	B(2)–N(4)–Li(2)	76.9(1)	79.2(4)
Li(2)–N(3)–C(19)	134.0(1)	135.0(4)	M(1)–N(4)–C(29)	134.45(9)	134.7(3)

The boron atoms in **6a** and **6c** exhibit distorted trigonal-planar geometries with substantial deviations from the ideal bond angles, although the sum of the angles is 360° in each case. The geometry about the nitrogen atoms is distorted tetrahedral (bond angle ranges: *ca*. 77–135°) with the smallest values associated with the B–N–Li angle. The NBN angles in **6a** and **6c** are equal within experimental error, while the B–N distances are intermediate between those of single- and double-bond values.[20] The geometry about the central metal atom is distorted tetrahedral [bond angle range: M = Mg: 67.54(5)–138.54(5)°; M = Zn; 68.4(2)–136.6(2)°] as a result of geometric constraints imposed by the *bam* ligands. The metal–nitrogen bond distances observed in complexes **6a** and **6c** are typical for Mg–N and Zn–N single bonds.[21]

The X-ray structural analysis of {[PhB(μ_3-N^{t}Bu)$_2$](Mg^{t}Bu)$_2$(μ_3-Cl)Li(OEt$_2$)$_3$} (**8**) reveals that each nitrogen atom of the *bam* ligand coordinates to two magnesium *tert*-butyl groups. The molecular geometry and atomic numbering scheme for **8** are shown in Figure 2, while pertinent structural parameters are summarized in Table 2. The Mg–N bond distances are equal within experimental error (*ca*. 2.13 Å), *cf*., *ca*. 2.09 Å in the spirocyclic complex **6a**. The magnesium atoms in the dimagnesiated derivative {[PhB(μ-

$N^tBu)_2](Mg^tBu)_2\}$ are also bridged by the chloride ion of a $ClLi(OEt_2)_3$ molecule. The structure of **8** is reminiscent of the framework observed for the dilithiated complex **3**,[11d] with the bridging THF ligand in **3** replaced by $ClLi(OEt_2)_3$ in **8**.

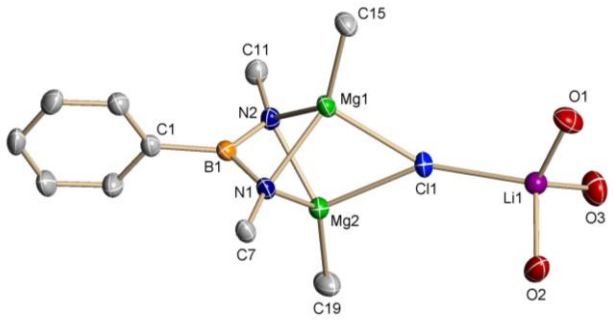

Figure 2. Thermal ellipsoid plot of $\{[PhB(\mu_3\text{-}N^tBu)_2](Mg^tBu)_2(\mu_3\text{-}Cl)Li(OEt_2)_3\}$ (**8**). For clarity, H atoms are omitted and only the α-carbons of the ^{t}Bu substituents and oxygen atoms of the Et_2O molecules are shown.

The mean B–N bond distances [1.451(3) Å] in **8** are equal within experimental error, *cf*., |d(B-N)| =1.446(4) Å in **3**. While the Li–O distances involving the bridging THF molecule in **3** are significantly different [2.270(7) and 2.013(6) Å], the chloride ion in **8** bridges the magnesium atoms symmetrically [2.536(1) Å, Mg(1)–Cl(1); 2.530(1) Å, Mg(2)–Cl(1)]. The lithio *am* complex $Li[^nBuC(N^tBu)_2]$ has been shown to entrap LiX salts to form complexes such as $\{(Li[^nBuC(N^tBu)_2])_2{\cdot}LiCl{\cdot}THF\}_2$.[22]

The boron atom in **8** exhibits a distorted trigonal-planar geometry [Σ∠ 360.0(2)°], while the magnesium atoms adopt distorted tetrahedral geometries [bond angle range *ca*. 66–138.5°] with the smallest angles associated with the N–Mg–N angle. The NBN angle [105.6(2)°] in **8** is similar to those in **6a** (*ca*. 107°), but significantly smaller than that in **3** [111.4(3)°].[11d] The larger angle in the latter presumably reflects the accommodation of

the bulkier NDipp groups in **3**. As a result of the two four-coordinate nitrogen centers, the two four-membered N–B–N–Mg rings in **8** are puckered in a manner similar to that observed for **6a**.

Table 2. Selected Bond Lengths (Å) and Bond Angles (°) for {[PhB(μ_3-N^{t}Bu)$_2$](Mg^{t}Bu)$_2$(μ_3-Cl)Li(OEt$_2$)$_3$} (**8**).

Mg(1)–N(1)	2.139(2)	Mg(2)–N(1)	2.131(2)
Mg(1)–N(2)	2.132(2)	Mg(2)–N(2)	2.129(2)
Mg(1)–Cl(1)	2.536(1)	Mg(2)–Cl(1)	2.530(1)
Mg(1)–C(15)	2.131(3)	Mg(2)–C(19)	2.138(3)
B(1)–N(1)	1.446(3)	B(1)–N(2)	1.456(3)
N(2)–Mg(1)–N(1)	65.53(8)	N(2)–Mg(2)–N(1)	65.73(8)
N(1)–Mg(1)–Cl(1)	95.36(6)	N(1)–Mg(2)–Cl(1)	95.76(7)
N(1)–Mg(1)–C(15)	138.9(1)	N(1)–Mg(2)–C(19)	137.8(1)
C(15)–Mg(1)–Cl(1)	115.37(8)	C(19)–Mg(2)–Cl(1)	115.11(9)
N(1)–B(1)–N(2)	105.6(2)	N(1)–B(1)–C(1)	126.7(2)
N(2)–B(1)–C(1)	127.7(2)		

The X-ray structure of {[PhB(μ-NDipp)$_2$]Mg(OEt$_2$)$_2$} (**10**) shows that the [PhB(NDipp)$_2$]$^{2-}$ ligand is coordinated to a single Mg^{2+} cation in an *N*,*N*'-chelated fashion. The coordination sphere is completed by oxygen atoms from two THF molecules. The molecular geometry and atomic numbering scheme are shown in Figure 3, while pertinent structural parameters are summarized in Table 3.

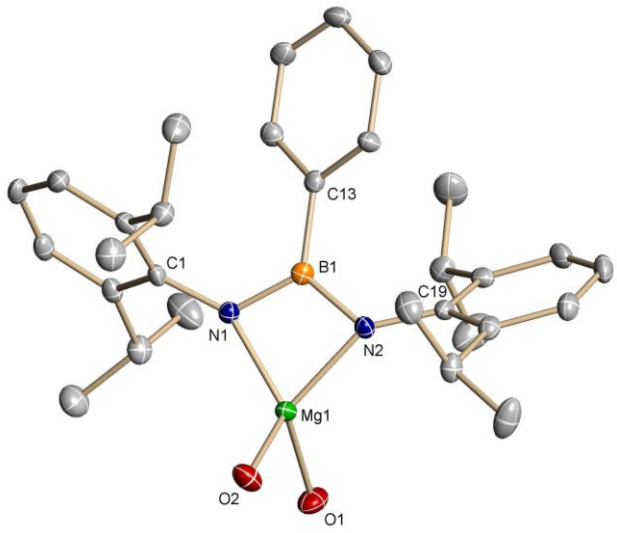

Figure 3. Thermal ellipsoid plot of {[PhB(μ-NDipp)$_2$]Mg(OEt$_2$)$_2$} (**10**). For clarity, H atoms are omitted and only the oxygen atoms of the Et$_2$O molecules are shown.

Table 3. Selected Bond Lengths (Å) and Bond Angles (°) for {[PhB(μ-NDipp)$_2$]Mg(OEt$_2$)$_2$} (**10**).

Mg(1)–N(1)	1.985(3)	Mg(1)–N(2)	1.973(3)
Mg(1)–O(1)	2.017(3)	Mg(1)–O(2)	2.015(3)
B(1)–N(1)	1.439(5)	B(1)–N(2)	1.449(5)
N(1)– Mg(1)–O(1)	129.7(1)	N(1)–Mg(1)–O(2)	117.4(1)
N(1)–Mg(1)–N(2)	74.7(1)	O(1)–Mg(1)–O(2)	96.4(1)
B(1)–N(1)–C(1)	125.4(3)	B(1)–N(2)–C(19)	125.7(3)
B(1)–N(1)–Mg(1)	86.3(2)	B(1)–N(2)–Mg(1)	86.4(2)
C(1)–N(1)–Mg(1)	147.4(2)	C(19)–N(2)–Mg(1)	145.2(2)
N(1)–B(1)–N(2)	112.5(3)	N(2)–B(1)–C(13)	123.2(3)
N(1)–B(1)–C(13)	124.3(3)		

The Mg–N distances of *ca*. 1.98 Å in **10** are significantly shorter than those observed in the dimagnesiated complex **8** (*ca*. 2.13 Å). The formal 2+ charge on magnesium in **10** is a likely major contributor to the observed difference. The magnesium center in **10** adopts a distorted tetrahedral geometry [bond angle range: 74.7(1)–129.7(1)°] with the smallest angle associated with the N–Mg–N bond angle. The B–N distances [1.439(5) Å, B(1)–N(1); 1.449(5) Å, B(1)–N(2)] reflect substantial nitrogen–boron multiple-bond character.

The N–B–N bond angle of 112.5(3)° in **10** is larger than those observed in **6a** and **8** (*ca*. 107°), but similar to that in the dilithiated *bam* complex **3** [111.4(3)°].[11d] The larger NBN angles observed in **3** and **10** accommodate the bulkier NDipp groups in the *bam* ligand in these complexes. The geometries at the boron and nitrogen atoms of the $[PhB(NDipp)_2]^{2-}$ ligand in **10** are distorted trigonal planar [Σ∠(°): 360.0(3), B(1); 359.1(3), N(1); 357.3(3), N(2)]. The four-membered Mg(1)–N(2)–B(1)–N(1) ring is essentially planar [0.0040 Å mean dev.].

Syntheses and Characterization of Group 13 *bam* complexes. We have previously reported the syntheses and structural characterization of the monolithiated spirocyclic complexes $\{(Et_2O)\mu\text{-}Li[PhB(\mu\text{-}N^tBu)_2]_2M\}$ (**11b**, M = Ga; **11c**, M = In) by the reactions of **1a** with MCl_3 in a 2:1 molar ratio.[16] Attempts to prepare the analogous aluminum complex $\{(Et_2O)\mu\text{-}Li[PhB(\mu\text{-}N^tBu)_2]_2Al\}$ (**11a**) by this method were unsuccessful. Complex **11a** can be obtained, however, in a two-step process involving the initial preparation of the mono-*bam* complex $\{[PhB(\mu\text{-}N^tBu)_2]AlCl(OEt_2)\}$ (**12**), which can be isolated in 60% yield from the reaction of **1a** and $AlCl_3$ in a 1:1 molar ratio, followed by treatment of **12** with **1a** (Scheme 5).

Scheme 5

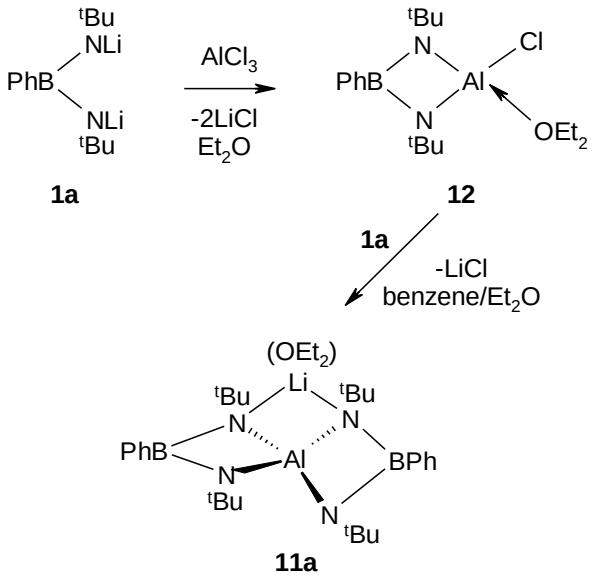

The structure of **12** was established by a single-crystal X-ray analysis (Figure 4), and pertinent structural parameters are summarized in Table 4.[23] Solvation of the aluminum centre by diethyl ether apparently prevents dimerization, *cf.*, the dimeric structure of the unsolvated complex {[PhB(μ_3-N^{t}Bu)(μ-N^{t}Bu)]GaCl}$_2$.[16] The geometry around the aluminum center in **12** is distorted tetrahedral [bond angle range: 79.99(4)–124.62(4)°]. The bond angle N–Al–N is acute [79.99(4)°], but larger than the mean value of 70.91(5)° observed for aluminum *am* complexes of the type RC(μ-NR')$_2$]AlCl$_2$ [R = Me, R' = ^{i}Pr; R = ^{t}Bu, R' = ^{i}Pr, Cy].[6b] The [PhB(μ-N^{t}Bu)$_2$]Al core in **12** forms a nearly planar metallacycle with an N(2)–Al(1)–N(1)–B(1) torsion angle of 3.05(7)°. The boron and three-coordinate nitrogen atoms exhibit distorted trigonal-planar coordination ($\Sigma\angle$ *ca*. 360°), the latter atoms displaying a larger disparity [bond angle range at B(1): 106.36(9)–128.5(1)°; bond angle range at N(1) and N(2): *ca*. 87–140°].

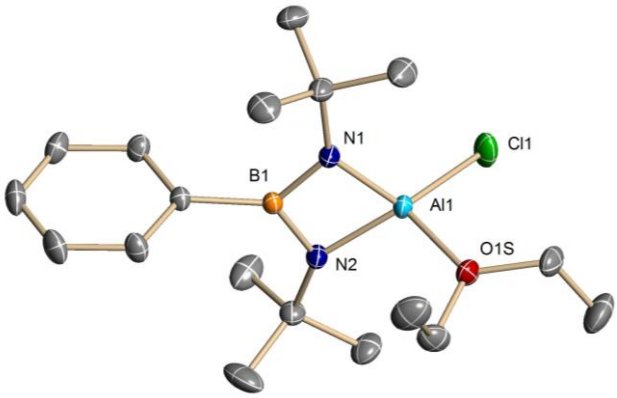

Figure 4. Thermal ellipsoid plot of {[PhB(μ-N^{t}Bu)$_2$]AlCl(OEt$_2$)} (**12**). For clarity, H atoms are omitted.

Table 4. Selected Bond Lengths (Å) and Bond Angles (°) for {[PhB(μ-N^{t}Bu)$_2$]AlCl(OEt$_2$)} (**12**).

Al(1)–Cl(1)	2.1402(5)	Al(1)–O(1)	1.8641(9)
Al(1)–N(1)	1.806(1)	Al(1)–N(2)	1.802(1)
B(1)–N(1)	1.442(2)	B(1)–N(2)	1.455(2)
N(1)-Al(1)–N(2)	79.99(4)	N(1)–Al(1)–Cl(1)	124.18(4)
N(1)–Al(1)–O(1)	115.05(5)	N(2)–Al(1)–Cl(1)	124.62(4)
B(1)–N(1)–C(10)	132.26(9)	B(1)–N(2)–C(20)	131.93(9)
B(1)–N(1)–Al(1)	86.83(7)	B(1)–N(2)–Al(1)	86.62(7)
C(10)–N(1)–Al(1)	140.19(8)	C(20)–N(2)–Al(1)	140.40(8)
N(1)–B(1)–C(1)	128.5(1)	N(2)–B(1)–C(1)	125.2(1)
N(1)–B(1)–N(2)	106.36(9)		

The Al–Cl distance of 2.1402(5) Å in **12** falls between those reported for aluminum mono- and bis-*am* complexes, *ca*. 2.10 and 2.19 Å, respectively.[6b] The B–N distances [1.442(2) and 1.455(2) Å] indicate significant multiple-bond character. The Al–N bond lengths [1.806(1) and 1.802(1) Å] are shorter by *ca*. 0.07 Å than the Al–N distances in related mono-*am* complexes,[6b] presumably as a result of the dianionic charge of the *bam* ligand in **12**. There are no intermolecular Al···Cl interactions present in the unit cell of **12**.

The reaction of **12** with **1a** in a 1:1 molar ratio in boiling benzene in the presence of a small amount of diethyl ether produces {$(Et_2O)\mu$-Li[PhB(μ-N^{t}Bu)$_2$]$_2$Al} (**11a**) in 33 % yield (Scheme 6). The multinuclear NMR spectra of **11a** are consistent with a spirocyclic structure similar to that previously established for **11b** and **11c**.[16] The ^{1}H NMR spectrum of **11a** in C_6D_6 shows resonances for the Ph and N^{t}Bu groups, in addition to the coordinated Et_2O molecule, with the appropriate relative intensities. The ^{1}H and ^{13}C NMR spectra of **11a** in C_6D_6 at room temperature reveal the equivalence of all four N^{t}Bu environments indicative of a fluxional process involving the lithium center, as observed for **11b** and **11c**.[16] The ^{27}Al, ^{11}B, and ^{7}Li NMR spectra of **11a** exhibit singlets at δ 488.2, 36, and 0.89, respectively.

In an attempt to synthesize the boron analogue of **11a**, the reaction of **1a** with $BF_3\cdot OEt_2$ in a 2:1 molar ratio was investigated. The ^{1}H and ^{11}B NMR spectra recorded as a function of time revealed the existence of more than one reaction pathway. The initial observation of two equally intense resonances at δ 43 and 30 in the ^{11}B NMR spectrum (indicative of inequivalent three-coordinate boron environments), associated with ^{t}Bu and Ph resonances with relative intensities of 18:5 in the ^{1}H NMR spectrum, is attributed to

the formation of the complex [PhB(μ-N^{t}Bu)$_2$]BF (**13**) (Scheme 6). Subsequently, the generation of the spirocyclic complex **11d** is indicated by the appearance of a broad resonance at δ 22 and a sharp singlet at δ 0 in the ^{11}B NMR spectrum (approximate intensity ratio 2:1), indicative of three- and four-coordinate boron environments, respectively.[19] The borazine [PhF$_2$B$_3$N$_3$^{t}Bu$_3$] (**14**) has been isolated from this reaction and identified by X-ray crystallography and multinuclear NMR spectra.[24] The NMR resonances for **14** grow at the expense of those attributed to **13** during the course of the reaction, and the formation of **14** is favored relative to **11d** when the reaction is carried out on a 1:1 molar ratio. A possible route to **14** involving the cyclodimerization of **13** to an eight-membered ring **15** is shown in Scheme 6.[25] However, in view of the known stability of related B$_4$N$_4$ rings, *e.g.*, (ClBN^{t}Bu)$_4$, the direct formation of **14** from **13** cannot be ruled out.

Scheme 6

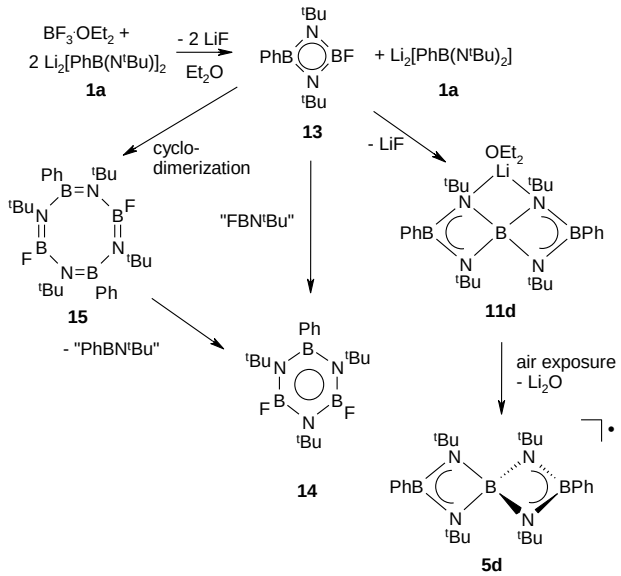

EPR and DFT Investigations of Early Main-Group Element and Zn *bam* Radicals. In a preliminary communication, we described the one-electron oxidation of the spirocyclic anions **4a** and **4b** to give the stable neutral radicals **5a** (dark red) and **5b** (dark green) (Scheme 1).[17,18] In this work, we discuss the characterization of the indium and boron analogues, **5c** and **5d**, respectively.

The oxidation of **11c** with one-half of an equivalent of iodine generates a dark green solution of complex **5c** (Figure 5) that, in contrast to **5a** and **5b**, is unstable at ambient temperature. Thus the oxidation was carried out at −78°C, and the paramagnetic species formed were investigated by variable-temperature (VT) EPR spectroscopy. The bright purple solutions of complex **5d** (Figure 5) formed by air oxidation of the products of the reaction of **1a** with $BF_3{\cdot}OEt_2$ in a 2:1 molar ratio (*vide supra*) were also investigated by EPR spectroscopy. Whereas the intense dark green color of **5c** lasts only for minutes at room temperature,[27] diethyl ether solutions of radical **5d** remain dark purple and exhibit similar EPR spectra even after two years.

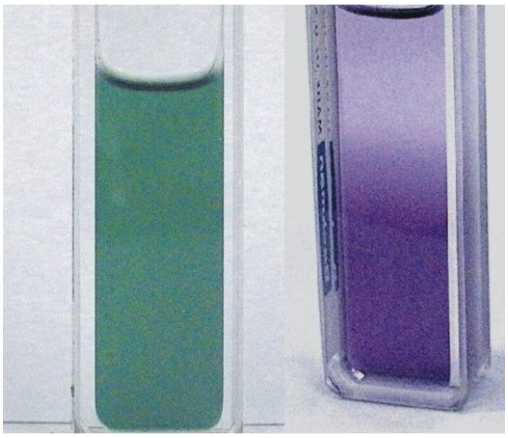

Figure 5. Photographs of diethyl ether solutions of the *neutral* spirocyclic radicals $\{[PhB(\mu\text{-}N^tBu)_2]_2M\}^\bullet$ (left, M = In, **5c**; right, M = B, **5d**).

Theoretical calculations were first carried out on the D_{2d}-symmetric diamagnetic model systems $\{[PhB(\mu\text{-}NMe)_2]_2M\}^-$ (M = In, B) to evaluate their frontier orbitals. The HOMOs (highest-occupied molecular orbitals) of these diamagnetic anions are non-degenerate and exhibit equal delocalization of spin density over all four nitrogen centers. Thus, like **5a** and **5b**, the corresponding spirocyclic radicals $\{[PhB(\mu\text{-}N^tBu)_2]_2In\}^\bullet$ (**5c**) and $\{[PhB(\mu\text{-}N^tBu)_2]_2B\}^\bullet$ (**5d**) are expected to retain the D_{2d} symmetry of their parent diamagnetic anions in solution. The calculated structures for the model radicals $\{[PhB(\mu\text{-}NMe)_2]_2M\}^\bullet$ (M = In, B) can be compared to the structures determined for the analogous aluminum and gallium systems by X-ray crystallography.[17] As expected, the M–N bond lengths in M = In and B derivatives are considerably longer (2.073 Å) and shorter (1.532 Å), respectively, than the corresponding bond lengths in M = Al or Ga derivatives.[17] The geometries of the two MNBN rings are close to square planar in the all-boron system $\{[PhB(\mu\text{-}NMe)_2]_2B\}^\bullet$ (bond angle range: *ca*. 85–97°), whereas the indium analogue displays distinctly asymmetric InNBN rings with very acute N–In–N bond angles (68°); the geometries of the MNBN rings in the M = Al and Ga derivatives fall between the values calculated for the indium and boron systems.[17] These differences in binding of the two *bam* ligands to the central atom reflect the different sizes of the Group 13 elements M = B, Al, Ga, In.

Considering the composition of the SOMO (singly-occupied molecular orbital) of the model radicals $\{[PhB(\mu\text{-}NMe)_2]_2M\}^\bullet$, the experimental EPR spectra of both **5c** and **5d** will exhibit hyperfine structure due to interaction of the unpaired electron with four equivalent nitrogen (^{14}N, I = 1, 99.6 %) centers. In addition, hyperfine structure due to the central metal (**5c**: ^{113}In, $I = {}^9/_2$, 4.3 %; ^{115}In, $I = {}^9/_2$, 95.7 %; **5d**: ^{10}B, I = 3, 19.9 %; ^{11}B, I =

$^3/_2$, 80.1 %) and two equivalent boron atoms of the *bam* ligands may be observed due to spin polarization effects. The experimental EPR spectra of **5c** obtained at –40 °C and **5d** obtained at 25 °C are shown in Figures 6a and 7a, respectively. The experimental EPR spectra are best simulated by assuming interactions of the unpaired electron with the central main group element, four equivalent nitrogen centers, and two equivalent boron atoms. The simulations shown in Figures 6b and 7b for **5c** and **5d**, respectively, were obtained by using the hyperfine coupling (hfc) constants given in Table 5, in which there is a fairly good agreement between the experimental and the calculated hfc values (Table 5). Hence, the experimental and simulated EPR spectra, together with DFT calculations, indicate that the neutral radicals {[PhB(μ-N^{t}Bu)$_2$]$_2$In}$^\bullet$ (**5c**) and {[PhB(μ-N^{t}Bu)$_2$]$_2$B}$^\bullet$ (**5d**) adopt spirocyclic structures in solution as depicted in Scheme 1.

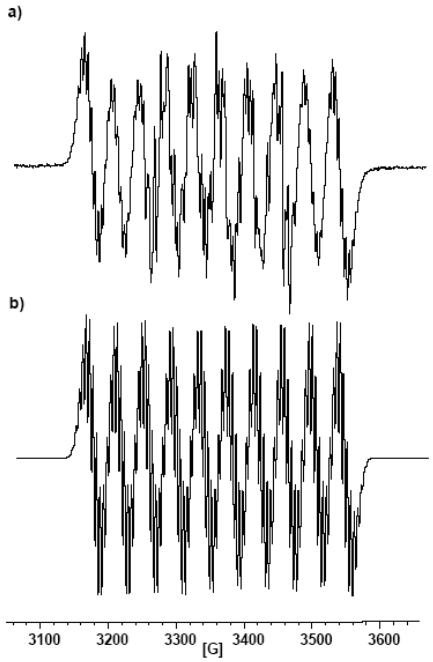

Figure 6. Experimental (a) and simulated (b) X-band EPR spectra of a diethyl ether solution of {[PhB(μ-N^{t}Bu)$_2$]$_2$In}$^\bullet$ (**5c**) at –40 °C.

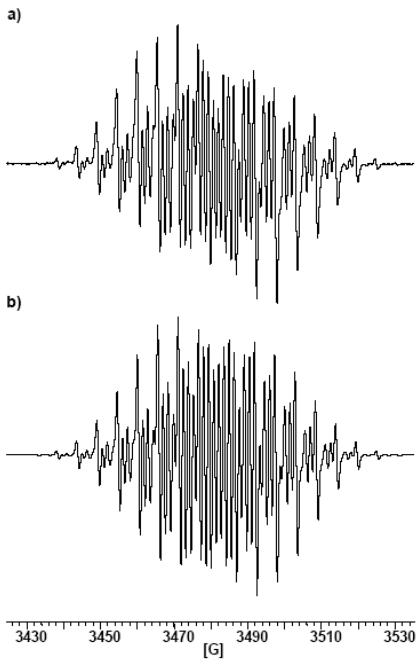

Figure 7. Experimental (a) and simulated (b) X-band EPR spectra of a diethyl ether solution of {[PhB(μ-N^{t}Bu)$_2$]$_2$B}$^\bullet$ (**5d**) at 25 °C.

Table 5. Experimental and Calculated Hyperfine Coupling Constants [G] for {[PhB(μ-NR')$_2$]$_2$M}$^\bullet$ (M = In, B; R' = ^{t}Bu, Me).[a]

{[PhB(μ-NR')$_2$]$_2$M}$^\bullet$	**isotope**	**n**[b]	**exptl.** (R' = ^{t}Bu)	**calc.** (R' = Me)
M = In	^{113}In / ^{115}In	1	22.50 / 41.00	*c*
	^{14}N	4	4.70	4.10
	^{10}B / ^{11}B	2	1.70 / 5.18	–2.03 / –6.10
M = B	^{10}B / ^{11}B	1	2.31 / 6.92	–2.81 / –8.43
	^{14}N	4	5.46	4.59
	^{10}B / ^{11}B	2	1.85 / 5.56	–2.21 / –6.64

[a] Parameters were determined from simulations optimized to match the experimental spectra. 100 % Lorentzian line shapes. g = 2.00407, M = In; g = 2.00405, M = B.

[b] Number of nuclei.

[c] Unavailable (see Experimental Section).

The oxidation of the dilithiated Mg or Zn spirocyclic bis-*bam* complexes **6a** and **6c** (Scheme 7) was also investigated by EPR spectroscopy. Addition of one-half of an equivalent of iodine to colorless solutions of **6a** or **6c** in diethyl ether at room temperature generates persistent pink or bright purple solutions, respectively (Figure 8). DFT calculations for the neutral radicals $\{(Et_2O)Li[PhB(\mu\text{-}N^tBu)_2]_2M\}^\bullet$ (**16a**, M = Mg; **16b**, M = Zn) predict C_s-symmetric structures and localized spin density on the *bam* ligand that is not coordinated to Li^+ (see Scheme 7 and Figure 9). Consequently, the EPR spectra of both radicals are expected to show hyperfine structure resulting from interaction of the unpaired electron with two inequivalent nitrogen atoms. In addition, hyperfine structure arising from interactions with the central metal (**16a**: ^{25}Mg, $I = {}^5/_2$, 10 %; **16b**: ^{67}Zn, $I = {}^5/_2$, 4.1 %), one boron atom, and minor contributions from the adjacent *bam* ligand, *i.e.*, two equivalent nitrogen atoms and/or one boron atom, is expected due to spin polarization effects.

Scheme 7

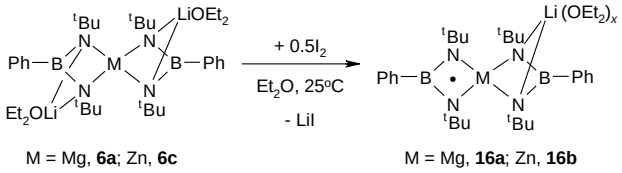

Figure 8. Photograph of diethyl ether solutions of the radicals {(Et_2O)Li[PhB(μ-$N^tBu)_2]_2M$}$^\bullet$ (left, M = Mg, **16a**; right, M = Zn, **16b**).

The experimental EPR spectrum obtained at room temperature for **16b** is shown in Figure 10a; the spectrum for **16a** exhibits a similar pattern owing to the low natural abundance of the spin-active isotopes for magnesium and zinc. Excellent simulations (Figure 10b) were obtained by using the hfc constants given in Table 6. The experimental and calculated hfc values are in close agreement. Hence, for both radicals, the EPR spectra support the prediction from DFT calculations that the unpaired electron is localized on one *bam* ligand. The EPR spectra for the zinc radical **16b** reveal minor interactions with the adjacent *bam* ligand, as well as some low-intensity satellites due to coupling of the unpaired electron to the ^{67}Zn nucleus.

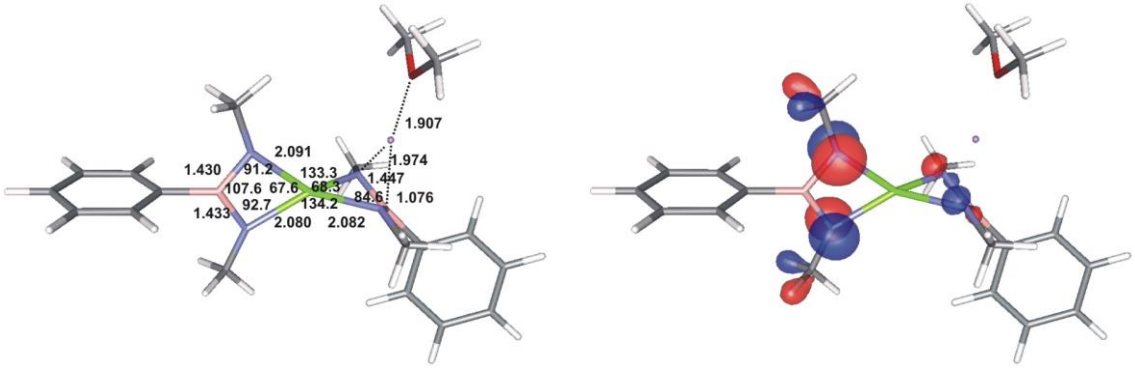

Figure 9. Optimized structure (left; bond lengths in Å, bond angles in deg.) and SOMO (right; isosurface values ± 0.06) of {(Me_2O)Li[PhB(μ-NMe)$_2$]$_2$Mg}$^\bullet$.

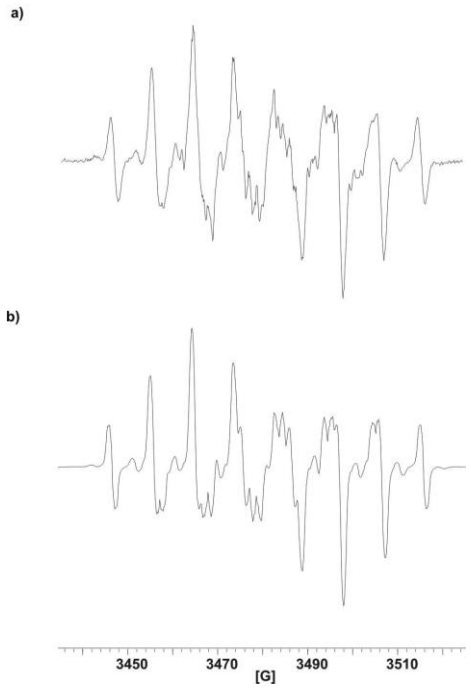

Figure 10. Experimental (a) and simulated (b) X-band EPR spectra of a diethyl ether solution of {(Et_2O)Li[PhB(μ-N^{t}Bu)$_2$]$_2$Zn}$^\bullet$ (**16b**) at 25 °C.

Table 6. Experimental and Calculated Hyperfine Coupling Constants [G] for $\{(Et_2O)Li[PhB(\mu\text{-}NR')_2]_2M\}^\bullet$ (M = Mg, Zn; R' = ^{t}Bu, Me).[a]

$\{(Et_2O)Li[PhB(\mu\text{-}NR')_2]_2M\}^\bullet$	**isotope**	**n**[b]	**exptl.** (R' = ^{t}Bu)	**calc.** (R' = Me)
M = Mg	^{10}B / ^{11}B	1	3.55 / 10.64	–4.01 / –12.30
	^{14}N	1	8.30	7.28
	^{14}N	1	8.55	7.89
	^{25}Mg	1	1.70	1.85
	^{10}B / ^{11}B	1	*a*[c]	–0.02
	^{14}N	2	*a*	–0.11
	^{7}Li	1	*a*	–0.01
M = Zn	^{10}B / ^{11}B	1	3.61 / 10.70	–4.06 / –12.19
	^{14}N	1	9.15	7.97
	^{14}N	1	9.34	8.36
	^{67}Zn	1	8.80	–7.82
	^{10}B / ^{11}B	1	*a*	–0.01
	^{14}N	2	0.45	–0.23
	^{7}Li	1	*a*	–0.03

[a] Parameters were determined from simulations optimized to match the experimental spectra. 100 % Lorentzian line shapes. g = 2.00446, M = Mg; g = 2.00526, M = Zn. [b] Number of nuclei. [c] *a* indicates no observable hfc constant.

The first indications of the formation of paramagnetic early main-group metal *bam* complexes came from investigations of lithium derivatives of the type **1**.[11c] It was observed that the initially colorless solutions of **1a**–**c** became red upon exposure to air. In preliminary EPR studies, only coupling to two equivalent ^{14}N nuclei (a five-line pattern) was resolved. In the absence of resolved coupling to ^{7}Li centers, it was not possible to speculate on the state of aggregation of the radical species.[11c]

We have now carried out the oxidation of **1a** with one-half of an equivalent of iodine in diethyl ether at room temperature (Scheme 8). The bright pink species so

formed is unstable at room temperature. Consequently, the solutions used for VT EPR studies were prepared at −78 °C. The EPR spectrum obtained at −40 °C is shown in Figure 11a. This spectrum is best simulated (see Table 7) with hyperfine interactions of the unpaired electron with *one* lithium atom (^{7}Li, $I = {}^{3}/_{2}$, 92.41 %; ^{6}Li, $I = 1$, 7.59 %), two equivalent nitrogen centers, and one boron atom, suggesting the formation of the *monocyclic* radical {[PhB(μ-N^{t}Bu)$_2$]Li(OEt$_2$)$_x$}$^{\bullet}$ (**17**), in which the radical monoanion [PhB(N^{t}Bu)$_2$]$^{-\bullet}$ is chelated to a diethyl ether-solvated lithium center.

Scheme 8

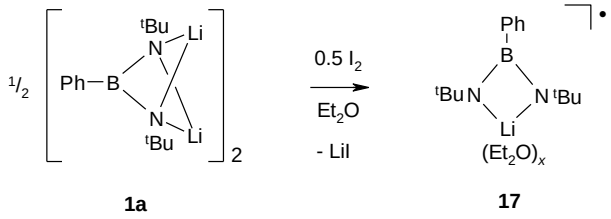

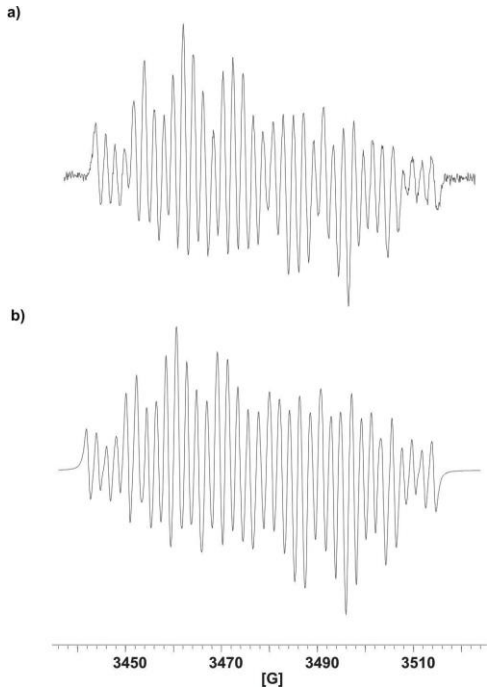

Figure 11. Experimental (a) and simulated (b) X-band EPR spectra of a diethyl ether solution of {[PhB(μ-N^{t}Bu)$_2$]Li(OEt$_2$)$_x$}$^{\bullet}$ (**17**) at −40 °C.

Table 7. Experimental and Calculated Hyperfine Coupling Constants [G] for {[PhB(μ-NR')$_2$]Li}$^\bullet$ (R' = ^{t}Bu, Me).[a]

{[PhB(μ-NR')$_2$]Li}$^\bullet$	Isotope	n[b]	exptl. (R' = ^{t}Bu)	calc. (R' = Me)
	^{10}B / ^{11}B	1	3.67 / 11.18	–4.24 / –12.72
	^{14}N	2	8.51	7.59
	^{7}Li	1	2.14	–2.39

[a] Parameters were determined from simulations optimized to match the experimental spectra. 100 % Lorentzian line shapes. g = 2.00443. [b] Number of nuclei.

The plausibility of the assignment of the experimental EPR spectrum to the monocyclic radical was supported by DFT calculations. Figure 12 shows the optimized structure and SOMO calculated for the model system {[PhB(μ-NMe)$_2$]Li(OEt$_2$)$_x$}$^\bullet$; the calculated hfc constants are listed in Table 7. The excellent match between the calculated and experimental values provides strong support for the identification of the transient radical as the monolithium species {[PhB(μ-N^{t}Bu)$_2$]Li(OEt$_2$)$_x$}$^\bullet$.

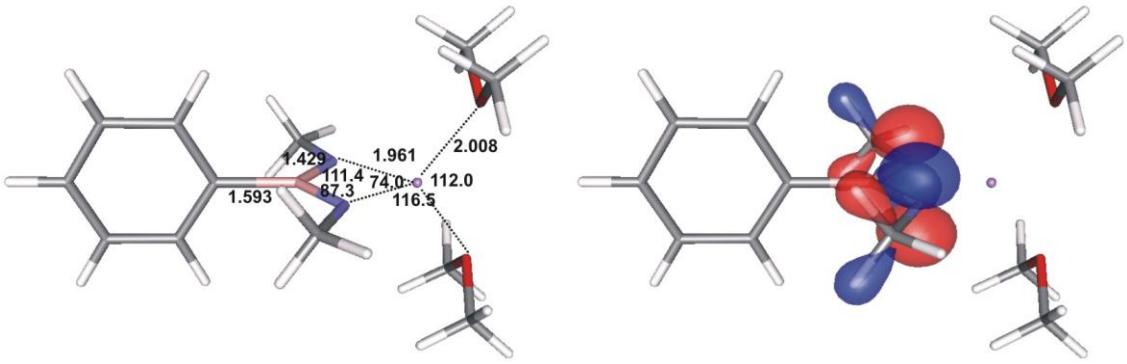

Figure 12. Optimized structure (left; bond lengths in Å, bond angles in deg.) and SOMO (right; isosurface values ± 0.06) of {[PhB(μ-NMe)$_2$]Li(OMe$_2$)$_2$}$^\bullet$.

Conclusions

A variety of magnesium complexes of the dianionic *bam* ligand have been synthesized and structurally characterized. These magnesium reagents offer a potential alternative to the widely used lithium derivatives for the transfer of *bam* ligands to other metal centers. In common with other early main-group metal *bam* complexes, these novel magnesium and zinc, complexes are readily oxidized to paramagnetic species. The one-electron oxidation of the metal-coordinated *bam* dianion $[PhB(\mu\text{-}N^tBu)_2]^{2-}$ to the corresponding radical anion $[PhB(N^tBu)_2]^{-\bullet}$ can be controlled by using the appropriate amount of iodine as the oxidizing agent. The combination of EPR spectroscopic analyses and DFT calculations provides information about both the molecular and electronic structures, *e.g.*, spin distribution, of these paramagnetic complexes in solution. Similar studies of complexes in which the radical anion $[PhB(N^tBu)_2]^{-\bullet}$ is coordinated to lithium or Group 13 metal centers indicate the qualitative trend in stabilities depicted in Chart 2.

Chart 2

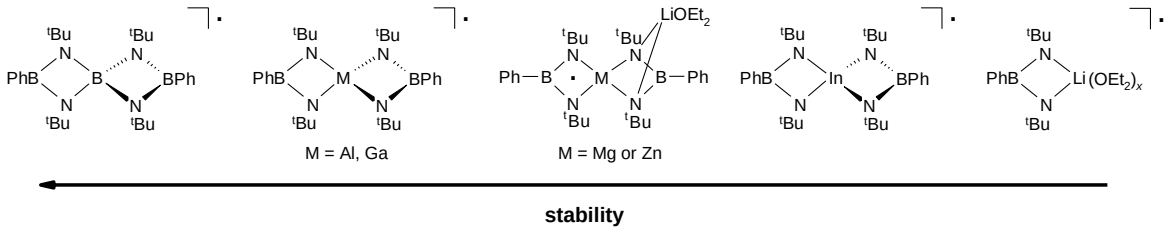

For the spirocyclic systems, the higher stability of the B, Al, and Ga-containing radicals compared to the Mg and Zn systems can be attributed to the delocalization of the unpaired electron over both *bam* ligands in the Group 13 complexes. The high stability of the boron-centered radical **5d** in solution is noteworthy. In contrast to **5a** and **5b**,

however, it has not yet been possible to devise a synthetic route that will allow the isolation of **5d** in the solid state. The lower stability of **5c** may result from a combination of stronger intermolecular, *i.e.*, radical-radical, interactions as a result of the larger In center and weaker In-N bonds compared to **5a**, **5b**, and **5d**. Intermolecular association to form larger aggregates is likely the reason for the low stability of the mononuclear Li complex.

These results suggest that redox behavior is an important feature of the chemistry of the *bam* ligand, as implied by the frequent observation of intensely colored solutions in the metathetical reactions of Li_2*bam* reagents with main-group element halides. This fundamental difference between the behavior of main-group metal complexes of *bam* ligands compared to that of *am* ligands undoubtedly stems from the dianionic charge in the former.

Experimental

Reagents and General Procedures. The compounds ^{t}BuMgCl (2.0 M solution in Et_2O), MesMgBr (1.0 M solution in Et_2O), ^{n}BuMgCl (2.0 M solution in Et_2O), MeMgBr (3.0 M solution in Et_2O), $MgCl_2$ (anhydrous beads, 10 mesh, 99.99 %), PhMgCl (2.0 M solution in THF), ^{i}PrMgCl (2.0 M solution in THF), $^{n/s}Bu_2Mg$ (1.0 M solution in heptane), and $BF_3{\cdot}OEt_2$ were commercial samples (Aldrich) and used as received. Anhydrous $ZnCl_2$ was prepared by heating $ZnCl_2{\cdot}H_2O$ under vacuum (150 °C, 10^{-2} Torr, 18 h). The reagents $AlCl_3$ and I_2 were sublimed prior to use.

The compounds $Li_2[PhB(\mu_3\text{-}N^tBu)_2]$ (**1a**),[11c] $PhB[N(H)Dipp]_2$,[11d] and $\{(Et_2O)\mu\text{-}Li[PhB(\mu\text{-}N^tBu)_2]_2In\}$ (**11c**)[16] were prepared by the literature methods.

Solvents were dried with appropriate drying agents and distilled onto molecular sieves before use. All reactions and the manipulation of moisture- and/or air-sensitive reagents or products were carried out under an atmosphere of argon or under vacuum using standard Schlenk techniques or a glovebox. All glassware was carefully dried prior to use.

Instrumentation. ^1H NMR spectra were recorded on Bruker AC 200 and DRX 400 spectrometers, and chemical shifts are reported relative to Me_4Si in $CDCl_3$. ^7Li, ^{11}B, ^{13}C, and ^{19}F NMR spectra were measured on a Bruker DRX 400 or a Bruker AMX2-300 spectrometer. All NMR spectra were obtained on C_6D_6 solutions at 25 °C. Chemical shifts are reported relative to those of $BF_3{\cdot}OEt_2$ in C_6D_6, Me_4Si in $CDCl_3$, 1.0 M LiCl in D_2O, and $CFCl_3$ in C_6D_6, respectively. Infrared spectra were obtained as Nujol mulls between KBr plates on a Nicolet Nexus 470 FT-IR spectrometer in the range 4000–350 cm^{-1}. Elemental analyses were provided by the Analytical Services Laboratory of the Department of Chemistry, University of Calgary. X-band EPR spectra were recorded on a Bruker EMX 113 spectrometer equipped with a variable-temperature accessory. EPR spectral simulations were carried out by using the XEMR v. 0.7[31a] and WINEPR SimFonia v. 1.25[31b] programs.

Preparation of $\{(Et_2O)\mu\text{-}Li[PhB(\mu\text{-}N^tBu)_2]\}_2Mg$ (6a). *Method 1.* A solution of ^tBuMgCl in Et_2O (2.0 M, 0.72 mL, 1.43 mmol) was added to a solution of **1a** (0.35 g, 1.43 mmol) in toluene (50 mL) at room temperature producing a white slurry that was stirred for 18 h. The reaction mixture was filtered and the solvent removed *in vacuo*. The

resulting residue was dissolved in Et_2O, and concentration of the solution followed by storage at room temperature for 30 min. afforded X-ray quality colorless crystals of **6a** (0.41 g, 0.63 mmol, 89 %). Complex **6a** was also prepared in the manner described above by using the Grignard reagents MesMgBr (1.0 M solution in Et_2O), ^{n}BuMgCl (2.0 M solution in Et_2O), or MeMgBr (3.0 M solution in Et_2O). *Method 2*. A solution of **1a** (0.75 g, 3.06 mmol) in Et_2O (100 mL) was added to solid $MgCl_2$ (0.15 g, 1.53 mmol) at −78 °C producing a dark burgundy reaction mixture, which was allowed to warm to room temperature over a period of 20 min then set to reflux for 18 h. The resulting colorless solution was filtered and the solvent removed *in vacuo*. The residue was washed several times with cold *n*-hexane gave white amorphous **6a** (0.74 g, 1.14 mmol, 75 %). A concentrated solution of **6a** in diethyl ether stored at −15 °C for 1 d provided colorless crystals suitable for X-ray diffraction studies. Anal. Calcd for $C_{36}H_{66}B_2Li_2MgN_4O_2$: C, 66.86; H, 10.29; N, 8.66. Found: C, 66.57; H, 10.86; N, 8.80. ^{1}H NMR: δ 7.96–7.20 (m, 10 H, $-C_6H_5$), 3.32 [q, 8 H, $(CH_3CH_2)_2O$], 1.47 [s, 18 H, $-C(CH_3)_3$], 1.32 [s, 18 H, $-C(CH_3)_3$], 0.98 [t, 12 H, $(CH_3CH_2)_2O$]. ^{11}B NMR: δ 38 (br s). ^{7}Li NMR: δ 1.44 (s). ^{13}C NMR: δ four resonances in the range 150.9–125.6 ($-C_6H_5$), 66.0 [$(CH_3CH_2)_2O$], 51.0 [$-C(CH_3)_3$], 38.3 [$-C(CH_3)_3$], 37.9 [$-C(CH_3)_3$], 15.1 [$(CH_3CH_2)_2O$].

Preparation of {(THF)μ-Li[PhB(μ-N^{t}Bu)$_2$]}$_2$Mg (6b). A solution of PhMgCl in THF (2.0 M, 0.33 mL, 0.66 mmol) was added to a solution of **1a** (0.16 g, 0.66 mmol) in toluene (25 mL) at room temperature producing a cloudy pale yellow mixture that was stirred for 18 h. The reaction mixture was filtered and the solvent was removed *in vacuo*. The residue was redissolved in THF and concentration of the solution followed by storage at −15 °C for 3 d afforded colorless crystals of **6b** (0.15 g, 0.23 mmol, 71 %).

Anal. Calcd for $C_{36}H_{62}B_2Li_2MgN_4O_2$: C, 67.28; H, 9.72; N, 8.71. Found: C, 66.98; H, 10.18; N, 8.66. ^{1}H NMR: δ 8.18–7.21 (m, 10 H, $-C_6H_5$), 3.33 [br s, 8 H, $O(CH_2)_2(CH_2)_2$], 1.49 [s, 18 H, $-C(CH_3)_3$], 1.35 [s, 18 H, $-C(CH_3)_3$], 1.14 [br s, 8 H, $O(CH_2)_2(CH_2)_2$]. ^{11}B NMR: δ 38 (br s). ^{7}Li NMR: δ 1.43 (s). ^{13}C NMR: δ four resonances in the range 150.0–127.5 ($-C_6H_5$), 69.3 [$O(CH_2)_2(CH_2)_2$], 51.0 [$-C(CH_3)_3$], 50.9 [$-C(CH_3)_3$], 38.1 [$-C(CH_3)_3$], 38.0 [$-C(CH_3)_3$], 25.6 [$O(CH_2)_2(CH_2)_2$]. Complex **6b** was also prepared in the manner described above by using the Grignard reagent ^{i}PrMgCl (2.0 M solution in THF).

Preparation of {(THF)μ-Li[PhB(μ-N^{t}Bu)$_2$]}$_2$Zn (6c). A solution of **1a** (0.27 g, 1.12 mmol) in Et_2O (100 mL) was added to solid $ZnCl_2$ (0.08 g, 0.56 mmol) at −78 °C producing a dark burgundy reaction mixture, which was allowed to warm to room temperature over a period of 20 min then set to reflux for 18 h. The mixture was filtered and the solvent removed *in vacuo*. The residue was washed several times with and cold *n*-hexane to give white amorphous **6c** (0.20 g, 0.29 mmol, 51 %). Anal. Calcd for $C_{36}H_{66}B_2Li_2N_4O_2Zn$: C, 62.86; H, 9.67; N, 8.15. Found: C, 62.28; H, 9.98; N, 8.12. ^{1}H NMR: δ 7.74–7.20 (m, 10 H, $-C_6H_5$), 3.36 [q, 8 H, $(CH_3CH_2)_2O$], 1.39 [s, 36 H, $-C(CH_3)_3$], 0.98 [t, 12 H, $(CH_3CH_2)_2O$]. ^{11}B NMR: δ 37 (br s). ^{7}Li NMR: δ 1.16 (s). ^{13}C NMR: δ four resonances in the range 150.1–125.8 ($-C_6H_5$), 65.8 [$(CH_3CH_2)_2O$], 51.2 [$-C(CH_3)_3$], 37.6 [$-C(CH_3)_3$], 15.1 [$(CH_3CH_2)_2O$]. A concentrated solution of **6c** in Et_2O stored at −15 °C for 6 h provided colorless crystals that were suitable for X-ray diffraction studies.

Preparation of {[PhB(μ_3-N^{t}Bu)$_2$](Mg^{t}Bu)$_2$(μ_3-Cl)Li(OEt$_2$)$_3$} (8). A solution of ^{t}BuMgCl in Et_2O (2.0 M, 1.93 mL, 3.85 mmol) in toluene (10 mL) was added to a

solution of **1a** (0.47 g, 1.93 mmol) in toluene (50 mL) at room temperature producing a white slurry that was stirred for 18 h. The reaction mixture was filtered and the solvent was removed *in vacuo*. The residue was washed twice with cold *n*-hexane affording a pale yellow powder (0.58 g, 0.88 mmol, 46 %). A concentrated solution of **8** in diethyl ether (1 week, −15 °C) provided colorless X-ray quality crystals. Anal. Calcd for $C_{26}H_{51}BClLiMg_2N_2O$ (**8** − 2 Et_2O): C, 61.29; H, 10.09; N, 5.50. Found: C, 61.13; H, 10.81; N, 6.09. ^{1}H NMR: δ 7.57−6.99 (m, 5 H, $-C_6H_5$), 3.21 [q, 12 H, $(CH_3CH_2)_2O$], 1.44 [s, 18 H, $-C(CH_3)_3$], 1.12 [s, 18 H, $-C(CH_3)_3$], 0.86 [t, 18 H, $(CH_3CH_2)_2O$]. ^{11}B NMR: δ 39 (br s). ^{7}Li NMR: δ −0.37 (s). ^{13}C NMR: δ four resonances in the range 138.2−126.0 ($-C_6H_5$), 65.7 [$(CH_3CH_2)_2O$], 50.6 [$-C(CH_3)_3$], 36.9 [$-C(CH_3)_3$], 35.5 [$-C(CH_3)_3$], 21.8 [$-C(CH_3)_3$], 14.2 [$(CH_3CH_2)_2O$].

Preparation of {[PhB(μ_3-N^{t}Bu)$_2$](Mg^{i}Pr)$_2$(THF)$_2$} (9a). A solution of ^{i}PrMgCl in THF (2.0 M, 1.11 mL, 2.22 mmol) was added to a solution of **1a** (0.27 g, 1.11 mmol) in toluene (50 mL) at room temperature producing a white slurry that was stirred for 5 h. The reaction mixture was filtered to give a pale yellow filtrate from which the solvent was removed *in vacuo*. The residue was redissolved in Et_2O and concentrated to afford **9a** as colorless thin needle crystals (0.21 g, 0.41 mmol, 37 %). Anal. Calcd for $C_{24}H_{45}BMg_2N_2O$ (**9a** − 1 THF): C, 65.96; H, 10.38; N, 6.41. Found: C, 65.41; H, 10.76; N, 6.22. ^{1}H NMR: δ 7.87−7.25 (m, 5 H, $-C_6H_5$), 3.59 [br m, 8 H, $O(CH_2)_2(CH_2)_2$], 1.75 [d, 12 H, $-CH(CH_3)_2$, $^3J(^1H-^1H)$ = 8 Hz], 1.27 [br m, 8 H, $O(CH_2)_2(CH_2)_2$], 1.17 [s, 18 H, $-C(CH_3)_3$], 0.32 [septet, 2 H, $-CH(CH_3)_2$, $^3J(^1H-^1H)$ = 8 Hz]. ^{11}B NMR: δ 39 (br s). ^{13}C NMR: δ four resonances in the range 133.9−126.6 ($-C_6H_5$), 70.5 [$O(CH_2)_2(CH_2)_2$], 50.4

[–*C*(CH_3)$_3$], 37.2 [–C(*C*H_3)$_3$], 26.4 [O(CH_2)$_2$(*C*H_2)$_2$], 25.7 [–CH(*C*H_3)$_2$], 9.1 [–*C*H(CH_3)$_2$].

Preparation of {[PhB(μ_3-N^{t}Bu)$_2$](MgPh)$_2$(THF)$_2$} (9b). A solution of PhMgCl in THF (2.0 M, 0.60 mL, 1.21 mmol) was added to a solution of **1a** (0.15 g, 0.61 mmol) in toluene (50 mL) at room temperature producing a cloudy pale yellow reaction mixture that was stirred for 12 h. The reaction mixture was filtered isolating a pale yellow filtrate from which the solvent was removed *in vacuo*. The residue was washed twice with *n*-hexane affording **9b** as a yellow powder (0.23 g, 0.40 mmol, 66 %). Thin needle crystals of **9b** were isolated from a concentrated solution in Et_2O (9 d, –15 °C). Anal. Calcd for $C_{30}H_{41}BMg_2N_2O$ (**9b** – 1 THF): C, 71.34; H, 8.18; N, 5.55. Found: C, 70.88; H, 8.24; N, 5.82. ^{1}H NMR: δ 8.02–7.17 (m, 15 H, –C_6H_5), 3.60 [br m, 8 H, O(C*H*$_2$)$_2$(CH_2)$_2$], 1.33 [s, 18 H, –C(C*H*$_3$)$_3$], 1.09 [br m, 8 H, O(CH_2)$_2$(C*H*$_2$)$_2$]. ^{11}B NMR: δ 40 (br s). ^{13}C NMR: δ eight resonances in the range 166.3–125.8 (–*C*$_6$H$_5$), 70.0 [O(*C*H_2)$_2$(CH_2)$_2$], 50.7 [–*C*(CH_3)$_3$], 37.5 [–C(*C*H_3)$_3$], 25.4 [O(CH_2)$_2$(*C*H_2)$_2$].

Preparation of {[PhB(μ-NDipp)$_2$]Mg(OEt$_2$)$_2$} (10). A solution of $^{n/s}$Bu$_2$Mg in heptane (1.0 M, 3.16 mL, 3.16 mmol) was added to a solution of PhB[N(H)Dipp]$_2$ (1.39 g, 3.16 mmol) in *n*-hexane (150 mL) at –30 °C producing a red reaction mixture. The mixture was allowed to warm to room temperature over 20 min. and then set to reflux for 18 h. Concentration of the reaction mixture followed by layering with diethyl ether and cooling (–15 °C, 2 d) gave X-ray quality colourless crystals of **10** (0.62 g, 1.01 mmol, 32 %). Anal. Calcd for $C_{38}H_{59}BMgN_2O_2$: C, 74.70; H, 9.73; N, 4.58. Found: C, 74.11; H, 9.50; N, 4.29. ^{1}H NMR: δ 7.55–7.02 (m, 11 H, Ph and aryl of Dipp), 4.00 [septet, 4 H, –C*H*(CH_3)$_2$, ^3J(^{1}H–^{1}H) = 8 Hz], 3.16 [q, 8 H, (CH_3C*H*$_2$)$_2$O], 0.97 [d, 24 H, –CH(C*H*$_3$)$_2$,

$^{3}J(^{1}H–^{1}H)$ = 8 Hz], 0.73 [t, 12 H, (C*H*$_3$CH$_2$)$_2$O]. ^{11}B NMR: δ 31 (br s). ^{13}C NMR: δ eight resonances in the range 152.5–119.4 (Ph and aryl of Dipp), 67.1 [(CH$_2$*C*H$_2$)$_2$O], 35.1 [–*C*H(CH$_3$)$_2$], 22.9 [–CH(*C*H$_3$)$_2$], 14.6 [(*C*H$_2$CH$_2$)$_2$O]. IR (cm^{-1}): No N–H stretch.

Preparation of {[PhB(μ-N^{t}Bu)$_2$]AlCl(OEt$_2$)} (12). A colorless solution of **1a** (0.46 g, 1.86 mmol) in Et$_2$O (50 mL) was added to solid AlCl$_3$ (0.25 g, 1.86 mmol) cooled to –78 °C producing a bright purple reaction mixture. After 15 min., the stirred reaction mixture was allowed to reach room temperature affording a clear colorless solution. After an additional 15 min. at room temperature, a cloudy pale yellow reaction mixture was produced that was stirred for 8 h. The resulting mixture was filtered to remove LiCl. Removal of solvent *in vacuo* and addition of cold *n*-hexane gave a pale yellow precipitate of **12** (0.41 g, 1.11 mmol, 60 %) that was washed twice with cold *n*-hexane. Anal. Calcd for C$_{14}$H$_{23}$AlClBN$_2$: C, 58.95; H, 9.07; N, 7.64. Found: C, 58.42; H, 9.25; N, 7.72. ^{1}H NMR: δ 7.63 (d, 2 H, –C$_6$H$_5$), 7.24 (m, 3 H, –C$_6$H$_5$), 3.76 [q, 4 H, (CH$_3$C*H*$_2$)$_2$O], 1.22 [s, 18 H, –C(C*H*$_3$)$_3$], 0.81 [t, 6 H, (C*H*$_3$CH$_2$)$_2$O]. ^{11}B NMR: δ 36 (br s). ^{13}C NMR: δ 155.0 (–C$_6$H$_5$), 132.7 (–C$_6$H$_5$), 127.4 (–C$_6$H$_5$), 126.3 (–C$_6$H$_5$), 66.4 [(CH$_3$*C*H$_2$)$_2$O], 49.7 [–*C*(CH$_3$)$_3$], 35.6 [–C(*C*H$_3$)$_3$], 15.8 [(*C*H$_3$CH$_2$)$_2$O]. X-ray quality crystals of **12** were isolated from a concentrated solution in Et$_2$O (1 d, –15 °C).

Preparation of {[PhB(μ-N^{t}Bu)$_2$]$_2$In}$^\bullet$ (5c). A solution of I$_2$ in Et$_2$O (0.60 mL, 0.0643 M, 0.038 mmol) was added to a colorless solution of {(Et$_2$O)μ-Li[PhB(μ-N^{t}Bu)$_2$]$_2$In} (**11c**) (0.050 g, 0.076 mmol) in Et$_2$O (15 mL) at –80 °C instantly producing a dark green solution. The reaction mixture was kept at –80 °C prior to recording EPR spectra. UV-vis (Et$_2$O): λ_{max} = 481 (br), 646 nm (br).

Preparation of {(Et_2O)Li[PhB(μ-N^{t}Bu)$_2$]$_2$Mg}$^\bullet$ (16a). A solution of I_2 in Et_2O (0.70 mL, 0.024 M, 0.017 mmol) was added to a colorless solution of {(Et_2O)μ-Li[PhB(μ-N^{t}Bu)$_2$]}$_2$Mg (**6a**) (0.022 g, 0.034 mmol) in Et_2O (10 mL) at room temperature instantly producing a bright pink solution. The resulting reaction mixture was used for EPR studies. UV-vis (Et_2O): λ_{max} = 521 (br).

Preparation of {(Et_2O)Li[PhB(μ-N^{t}Bu)$_2$]$_2$Zn}$^\bullet$ (16b). A solution of I_2 in Et_2O (0.84 mL, 0.044 M, 0.037 mmol) was added to a colourless solution of {(Et_2O)μ-Li[PhB(μ-N^{t}Bu)$_2$]}$_2$Zn (**6c**) (0.051 g, 0.074 mmol) in Et_2O (10 mL) at room temperature instantly producing a bright purple solution. The resulting reaction mixture was studied by EPR spectroscopy. UV-vis (Et_2O): λ_{max} = 562 (br).

Preparation of {[PhB(μ-N^{t}Bu)$_2$]Li(OEt$_2$)$_x$}$^\bullet$ (17). A solution of I_2 in Et_2O (0.84 mL, 0.044 M, 0.037 mmol) was added to a colorless solution of Li_2[PhB(μ_3-N^{t}Bu)$_2$] (**1a**) (0.051 g, 0.074 mmol) in Et_2O (10 mL) at –80 °C instantly producing a pink solution. This solution was kept at –80 °C prior to recording EPR spectra.

X-ray Analyses

Relevant parameters for the data collections and crystallographic data are summarized in Table 8. Thermal ellipsoid plots are shown at the 30 % probability level and only selected carbon atoms are labeled.

Table 8. Selected Crystal Data and Data Collection Parameters for {(Et_2O)μ-Li[PhB(μ-N^{t}Bu)$_2$]}$_2$M (M = Mg, **6a**; M = Zn, **6c**), {[PhB(μ_3-N^{t}Bu)$_2$](Mg^{t}Bu)$_2$(μ_3-Cl)Li(OEt_2)$_3$} (**8**), {[PhB(μ-NDipp)$_2$]Mg(OEt_2)$_2$} (**10**), and {[PhB(μ-N^{t}Bu)$_2$]AlCl(OEt_2)} (**12**).[a]

	6a	**6c**	**8**	**10**[b]	**12**
formula	$C_{36}H_{66}B_2Li_2MgN_4O_2$	$C_{36}H_{66}B_2Li_2N_4O_2Zn$	$C_{34}H_{71}BClLiMg_2N_2O_3$	$C_{76}H_{118}B_2Mg_2N_4O_4$	$C_{18}H_{33}AlBClN_2O$
fw	646.74	687.80	657.75	1221.98	670.65
space group	$P2_1/n$	$P2_1/n$	$P\bar{1}$	$P\bar{1}$	$P2_1/n$
a, Å	9.977(2)	13.057(3)	10.142(2)	11.008(2)	11.8251(2)
b, Å	17.347(4)	17.268(4)	12.481(3)	17.524(4)	13.4014(2)
c, Å	24.129(5)	19.428(4)	18.091(4)	21.343(4)	14.6888(2)
α, deg	90	90	89.81(3)	111.85(3)	90
β, deg	92.00(3)	109.42(3)	81.72(3)	102.36(3)	106.965(1)
γ, deg	90	90	73.45	90.73(3)	90
V, Å^3	4173.3(1)	4131.4(1)	2170.4(7)	3713.4(2)	2226.48(6)
Z	4	4	2	2	4
d_{calcd}, g cm^{-3}	1.029	1.106	1.006	1.093	1.094
μ, mm^{-1}	0.075	0.627	0.146	0.081	0.218
F(000)	1416	1488	724	1336	792
R^c	0.0484	0.0749	0.0609	0.0754	0.0400
$R_w{}^d$	0.1166	0.1726	0.1548	0.1855	0.1137

[a]Temperature = 173(2) K; wavelength = 0.71073 Å. [b]The complex crystallizes with two independent but chemically-equivalent molecules in the asymmetric unit. [c]$R = \Sigma||F_o| - |F_c||/\Sigma|F_o|$ ($I > 2.00\sigma(I)$). [d]$R_w = \{[\Sigma w(F_o^2 - F_c^2)^2]/[\Sigma w(F_o^2)^2]\}^{1/2}$ (all data).

Computational Details

All calculations were done with the Gaussian 03 program.[29] The structures of all compounds were optimized in their ground states using density functional theory. Hybrid PBE0 exchange-correlation functional[30] and Ahlrichs' TZVP basis sets[31] were used in all optimizations (the corresponding ECP basis set was used for indium). Hyperfine coupling constants of paramagnetic species were calculated by single point calculations employing the optimized geometries, PBE0 functional, TZVP basis sets, and unrestricted Kohn-Sham formalism. For {[PhB(μ-NMe)$_2$]$_2$In}$^\bullet$, the use of a quasi-relativistic ECP for the heavier nucleus indium prevents the direct determination of its hfc constants using the applied method.

Acknowledgment. The authors gratefully acknowledge financial support from the Natural Sciences and Engineering Research Council (Canada), the Alberta Ingenuity Fund, Helsingin Sanomain 100-vuotissäätiö (H.M.T), and the University of Calgary.

Supporting Information Available: Full experimental details of the X-ray analyses. Crystallographic data in CIF format for complexes **6a**, **6c**, **8**, **10** and **12**. This material is available free of charge *via* the Internet at http://pubs.acs.org.

References

(1) For reviews, see: (a) Barker, J.; Kilner, M. *Coord. Chem. Rev*. **1994**, *133*, 219. (b) Edelmann, F.T. *Coord. Chem. Rev*. **1994**, *137*, 403.

(2) For examples, see: (a) Boeré, R. T.; Cole, M. L.; Junk, P. C. *New. J. Chem*. **2005**, *29*, 128. (b) Schmidt, J.A.R.; Arnold, J. *J. Chem. Soc., Dalton Trans*. **2002**, 2890. (c) Xia, A.; El-Kaderi, H.M.; Heeg, M.J.; Winter, C.H. *J. Organomet. Chem*. **2003**, *682*, 224. (d) Sadique, A.R.; Heeg, M.J.; Winter, C.H. *Inorg. Chem*. **2001**, *40*, 6349. (e) Srinivas, B.; Chang, C.C.; Chen, C.H.; Chiang, M.Y.; Chen. I.-T.; Wang, Y.; Lee, G.-H.; *J. Chem. Soc., Dalton Trans*. **1997**, 957. (f) Walther, D.; Gebhardt, P.; Fischer, R.; Kreher, U.; Görls, H. *Inorg. Chim. Acta*. **1998**, *281*, 181.

(3) For an example, see: Cotton, F.A.; Haefner, S.C.; Matonic, J.H.; Wang, X.; Murillo, C.A. *Polyhedron* **1997**, *16*, 541.

(4) For examples, see: (a) Chen, C.-T.; Huang, C.-A.; Tzeng, Y.-R.; Huang, B.-H. *J. Chem. Soc., Dalton Trans*. **2003**, 2585. (b) Kincaid, K.; Gerlach, C.P.; Giesbrecht, G.R.; Hagdorn, J.R.; Whitener, G,D,; Shafir, A.; Arnold, J. *Organometallics* **1999**, *18*, 5360.

(5) For an example, see: Li, M.-D.; Chang, C.C.; Wang, Y.; Lee, G.-H.; *Organometallics* **1996**, *15*, 2571.

(6) For examples, see: (a) Ergezinger, C.; Weller, F.; Dehnicke, K.Z. *Z. Naturforsch*. **1988**, *43b*, 1621. (b) Coles, M.P.; Swenson, D.C.; Jordan, R.F. *Organometallics* **1997**, *16*, 5183. (c) Coles, M.P.; Swenson, D.C.; Jordan, R.F. *Organometallics* **1998**, *17*, 4042. (d) Kottmair-Maieron, D.; Lechler, R.; Weidlein, J. *Z. Anorg. Allg. Chem*. **1991**, *593*, 111. (e) Lechler, R.; Hausen, H.-D.; Weidlein, J. *J. Organomet. Chem*. **1989**, *359*, 1. (f) Barker, J.; Blacker, N.C.; Phillips, P.R.; Alcock, N.W.; Errington, W.; Wallbridge, M.G.H. *J. Chem. Soc., Dalton Trans*. **1996**, 431.

(7) For an example, see: Duchateau, R.; Meetsma, A.; Teuben, J.H. *Chem. Commun*. **1996**, 223.

(8) For an example, see: Zhou, Y.; Richeson, D.S. *Inorg. Chem*. **1996**, *35*, 2448.

(9) For examples, see: (a) Hausen, H.-D.; Gerstner, F.; Shwarz, W. *J. Organomet. Chem*. **1978**, *145*, 277. (b) Zhou, Y.; Richeson, D.S. *Inorg. Chem*. **1996**, *35*, 1423.

(10) For an example, see: Doyle, D.; Gun'ko, Y.K.; Hitchcock, P.B.; Lappert, M.F. *J. Chem. Soc., Dalton Trans*. **2000**, 4093.

(11) (a) Fest, D.; Habben, C.D.; Meller, A.; Sheldrick, G.M.; Stalke, D.; Pauer, F. *Chem. Ber*. **1990**, *123*, 703. (b) Brask, J.K.; Chivers, T.; Schatte, G. *Chem. Commun*. **2000**, 1805. (c) Chivers, T.; Fedorchuk, C.; Schatte, G.; Brask, J.K. *Can. J. Chem*. **2002**, *80*, 821. (d) Chivers, T.; Fedorchuk, C.; Parvez, M. *Inorg. Chem*. **2004**, *43*, 2643. (e) Blais, P.; Brask, J. K.; Chivers, T.; Fedorchuk, C.; Schatte, G.; *ACS Symposium Series*, **2002**, *822*, 195.

(12) Armstrong, A. F.; Chivers, T.; Tuononen, H. M.; Parvez, M.; Boeré, R. T. *Inorg. Chem*, **2005**, *44*, 7981, and references therein.

(13) (a) Fuβstetter, H.; Nöth, H. *Chem. Ber*. **1979**, *112*, 3672. (b) Gudat, D.; Niecke, E.; Nieger, M.; Paetzold, P. *Chem. Ber*. **1988**, *121*, 565. (c) Heine, A.; Fest, D.; Stalke, D.; Habben, C.D.; Meller, A.; Sheldrick, G.M. *J. Chem. Soc., Chem. Commun*. **1990**, 742. (d) Habben, C.D.; Heine, A.; Sheldrick, G.M.; Stalke, D.; Bühl, M.; Schleyer, P.V.R. *Chem. Ber*. **1991**, *124*, 47. (e) Habben, C.D.; Herbst-Irmer, R.; Noltemeyer, M. *Z. Naturforsch*. **1991**, *46b*, 625. (f) Habben, C.D.; Heine, A.; Sheldrick, G.M.; Stalke, D. *Z. Naturforsch*. **1992**, *47b*, 1367. (g) Paetzold, P.; Hahnfeld, D.; Englert, U.; Wojnowski, W.; Dreczewski, B.; Pawelec, Z.; Walz, L. *Chem. Ber*. **1992**, *125*, 1073. (h) Koch, H.-J.; Roesky, H.W.; Besser, S.; Herbst-Irmer, R. *Chem. Ber*. **1993**, *126*, 571. (i) Geschwentner, M.; Noltemeyer, M.; Elter, G.; Meller, A. *Z. Anorg. Allg. Chem*. **1994**, *620*, 1403. (j) Chivers, T.; Gao, X.; Parvez, M. *Angew. Chem., Int. Ed. Engl*. **1995**, *34*, 2549. (k) Luthin, W.; Stratmann, J.-G.; Elter, G.; Meller, A.; Heine, A.; Gornitzka, H. *Z. Anorg. Allg. Chem*. **1995**, *621*, 1995. (l) Albrecht, T.; Elter, G.; Noltemeyer, M.; Meller, A. *Z. Anorg. Allg. Chem*. **1998**, *624*, 1514.

(14) Koch, H.-J.; Roesky, H.W.; Bohra, R.; Noltemeyer, M.; Schmidt, H.-G. *Angew. Chem., Int. Ed. Engl*. **1992**, *31*, 598.

(15) (a) Manke, D.R.; Nocera, D.G. *Inorg. Chim. Acta*. **2003**, *345*, 235. (b) Manke, D.R.; Nocera, D.G. *Inorg. Chem*. **2003**, *42*, 4431. (c) Manke, D.R.; Loh, Z.-H.; Nocera, D.G. *Inorg. Chem*. **2004**, *43*, 3618.

(16) Chivers, T.; Fedorchuk, C.; Schatte, G.; Parvez, M. *Inorg. Chem*. **2003**, *42*, 2084.

(17) Chivers, T.; Eisler, D.J.; Fedorchuk, C.; Schatte, G.; Tuononen, H.M.; Boeré, R.T. *Chem. Commun*. **2005**, 3930.

(18) The term "stable", as applied to radicals, is taken to indicate "a species that can be isolated and shows no sign of decomposition under an inert atmosphere at room temperature", whereas a "persistent" radical has "a relatively long lifetime under the conditions it is generated". Power, P.P. *Chem. Rev*. **2003**, *103*, 789.

(19) Nöth, H.; Wrackmeyer, B. In *Nuclear Magnetic Resonance Spectroscopy of Boron Compounds*; Springer-Verlag: Berlin, 1978; pp 74-101.

(20) Paetzold, P. *Phosphorus, Sulfur, Silicon*. **1994**, *93–94*, 39.

(21) For an example, see: Buijink, J.K.; Noltemeyer, M.; Edelmann, F.T. *Z. Naturforsch. Teil B* **1991**, *46*, 1328.

(21) A search for Mg–N distances in the Cambridge Structural Database provided 1,543 values with a mean of 2.13 Å and 948 distances in the range of 1.97–2.15 Å. Similarly, for Zn–N distances, 10,000 values were found, with a mean of 2.11 Å and 5174 distances in the range of 2.00–2.12 Å.

(22) Chivers, T.; Downard, A.; Parvez, M. *Inorg. Chem*. **1999**, *38*, 4347.

(23) Although complex **12** was mentioned in the preliminary communication,[17] no structural details were given.

(24) Chivers, T.; Fedorchuk, C.; Parvez, M. *Acta Crystallogr*. **2005**, *C61*, o47.

(25) The factors that determine the outcome of the cyclodimerization of B_2N_2 rings are not well understood. Gilbert, T.M.; Gailbreath, B.D. *Organometallics* **2001**, *20*, 4727.

(26) Bowser, J.R.; Neilson, R.H.; Wells, R.L. *Inorg. Chem*. **1978**, *17*, 1882.

(27) After a few minutes, the EPR spectrum of **5c** is replaced by an asymmetric spectrum indicating the presence of at least two radical species. The outer ends of this spectrum exhibit a pentet with 34 G width indicating hfc to two equivalent ^{14}N nuclei (A = 8.5 G). This pattern is repeated ten times suggesting coupling to a

single ^{115}In center. No coupling to boron was resolved. Although a possible candidate for this radical is the monocyclic *bam* complex [PhB(μ-N^{t}Bu)$_2$In]$^\bullet$, the calculated value of A^{115}_{In} for this radical is much higher than the observed value of ~ 21 G.

(28) (a) Eloranta, J. *XEMR*, version 0.7; University of Jyväskylä: Jyväskylä, Finland, 2004. (b) *WINEPR SimFonia*, version 1.25; Bruker Analytische: Messtechnik, Germany, 1996.

(29) Frisch, M. J.; Trucks, G. W.; Schlegel, H. B.; Scuseria, G. E.; Robb, M. A.; Cheeseman, J. R.; Montgomery, J. A.; Vreven, T.; Kudin, K. N.; Burant, J. C.; Millam, J. M.; Iyengar, S. S.; Tomasi, J.; Barone, V.; Mennucci, B.; Cossi, M.; Scalmani, G.; Rega, N.; Petersson, G. A.; Nakatsuji, H.; Hada, M.; Ehara, M.; Toyota, K.; Fukuda, R.; Hasegawa, J.; Ishida, M.; Nakajima, T.; Honda, Y.; Kitao, O.; Nakai, H.; Klene, M.; Li, X.; Knox, J. E.; Hratchian, H. P.; Cross, J. B.; Adamo, C.; Jaramillo, J.; Gomperts, R.; Stratmann, R. E.; Yazyev, O.; Austin, A. J.; Cammi, R.; Pomelli, C.; Ochterski, J. W.; Ayala, P. Y.; Morokuma, K.; Voth, G. A.; Salvador, P.; Dannenberg, J. J.; Zakrzewski, V. G.; Dapprich, S.; Daniels, A. D.; Strain, M. C.; Farkas, O.; Malick, D. K.; Rabuck, A. D.; Raghavachari, K.; Foresman, J. B.; Ortiz, J. V.; Cui, Q.; Baboul, A. G.; Clifford, S.; Cioslowski, J.; Stefanov, B. B.; Liu, G.; Liashenko, A.; Piskorz, P.; Komaromi, I.; Martin, R. L.; Fox, D. J.; Keith, T.; Al-Laham, M. A.; Peng, C. Y.; Nanayakkara, A.; Challacombe, M.; Gill, P. M. W.; Johnson, B.; Chen, W.; Wong, M. W.; Gonzalez, C.; Pople, J. A. Gaussian 03, (Revision C.02), Gaussian, Inc., Pittsburgh, PA, 2003.

(30) (a) Perdew, J. P.; Burke, K.; Ernzerhof, M., *Phys. Rev. Lett.* **1996**, *77*, 3865. (b) Perdew, J. P.; Burke, K.; Ernzerhof, M., *Phys. Rev. Lett.* **1997**, *78*, 1396. (c) Perdew, J. P.; Burke, K.; Ernzerhof, M., *J. Chem. Phys.* **1996**, *105*, 9982. (d) Ernzerhof, M.; Scuseria, G. E. *J. Chem. Phys.* **1999**, *110*, 5029.

(31) The basis sets were used as they are referenced in the Turbomole 5.7.1 internal basis set library. These basis sets can be downloaded from: ftp://ftp.chemie.uni-karlsruhe.de/pub/basen/ for free of charge. Site accessed, February 2005.